Journal of Molecular Liquids 398 (2024) 124244

Contents lists available at ScienceDirect

Journal of Molecular Liquids

journal homepage: www.elsevier.com/locate/molliq

An impact of inclined MHD on biviscosity Bingham hybrid nanofluid flow over porous stretching/shrinking sheet with heat transfer

U.S. Mahabaleshwar [a], S.M. Sachhin [a,*], L.M. Pérez [b], H.F. Oztop [c,d,e,*]

[a] Department of Studies in Mathematics, Shivagangothri, Davangere University, Davangere, India
[b] Departamento de Física, FACI, Universidad de Tarapacá, Casilla 7D, Arica 1000000, Chile
[c] Department of Mechanical and Nuclear Engineering, College of Engineering, University of Sharjah, 27272 Sharjah, United Arab Emirates
[d] Department of Mechanical Engineering, Technology Faculty, Firat University, Elazig, Turkey
[e] Department of Medical Research, China Med. University Hospital, China Med. University, Taichung, Taiwan

ARTICLE INFO

Keywords:
Hybrid nanofluids
Radiation
Inclined magnetic field
Porous
Heat source/sink

ABSTRACT

The present study examines the effect of radiation and inclined magnetic field on the biviscosity Bingham hybrid nanofluid flow on the permeable stretching/shrinking surface. Hybrid nano fluid composites are formed by dissolving Graphene oxide (*GO*) and Molybdenum disulfide (MoS_2) in base fluid Ethylene Glycol (*EG*), applying these nanoparticles to the Ethylene Glycol (base fluid) will enhance heat transfer. Furthermore, it studied the heat transmission process using variable thermal conductivity of the heat source/sink. Governing equations of velocity and temperature are converted to a set of nonlinear ordinary differential equations (ODE) via suitable transformations and the obtained equations are solved using the boundary conditions, energy equation with radiation, and heat source/sink effect solved analytically by using hypergeometric function. Significant physical characteristics like mass transpiration, Prandtl number, Biot number, and thermal radiations can be discussed using the graphical analysis. The investigation outcomes reveal that increasing the magnetic field enhances skin friction. Increasing the volume fraction, Biot number, and thermal radiation increases the thermal boundary layer, and velocity decreases by increasing the inverse Darcy parameter. Current work has many useful applications in engineering, biological and physical sciences, cleaning engine lubricants, thrust bearing technologies, etc.

1. Introduction

Hybrid nanofluid technology has advanced rapidly in recent years in a variety of engineering and science disciplines, including electronics and power generation where nanofluids are commonly obtained, due to these applications many researchers studied hybrid nanofluids such as Choi *et al.* [1] conducted research about nanoparticles by extracting heat conductivity over fluid flow. Thermal transfer through entropy analysis of hybrid nanofluid on a flat surface explored by Huminic *et al.* [2]. Das *et al.* [3] and Suresh *et al.* [4] studied the impact of heat conductivity in hybrid and regular nanofluids and features of diluted water-based hybrid nanofluids in terms of low-pressure with turbulence. Afterward, Siddiqui *et al.* [5] studied the heat transfer of an Al_2O_3-*Cu* hybrid nanofluid at different mixture ratios. Marangoni thermosolutal convection for hybrid nanofluid models explored by Mahabaleshwar *et al.* [6].

The movement effects of ferrofluids with geometric fields provide magnetic influences and influence the flow of heat-conducting fluid. MHD is the study of the behavior of electrically conducting fluids along with the magnetic field, due to numerous applications many researchers keen to study magnetic fields such as Rostami *et al.* [7] focused on the MWCNT-*CuO*/water hybrid nanofluid thermal conductivity and magnetohydrodynamics evaluation with artificial neural networks. Vishalakshi *et al.* [8] studied the effect of radiation and magnetohydrodynamics in mixed convection hybrid nanofluid flow across a stretched surface, the same was work extended with improved heat transfer using hybrid nanofluid comprising graphene Nanoplatelets and silver by Yarmand *et al.* [9].

The term porous medium refers to any substance that consists of a solid structure and an interconnected space. Numerous applied science as well as engineering fields make use of the idea of porous media, including purification, mechanics, acoustics, geomechanics, soil mechanics, rock mechanics, physics, biological science, and material

* Corresponding authors.
E-mail addresses: sachinsm030@gmail.com (S.M. Sachhin), hakanfoztop@firat.edu.tr (H.F. Oztop).

https://doi.org/10.1016/j.molliq.2024.124244
Received 29 August 2023; Received in revised form 3 February 2024; Accepted 9 February 2024
Available online 11 February 2024

Nomenclature

List of symbols	Descriptions (SI unit)
A_1, A_2, A_3, A_4, A_5	Constants [-]
Bi	Biot number [-]
C_p	Specific heat $[JK^{-1}Kg^{-1}]$
Da^{-1}	Inverse Darcy factor [-]
f	Velocity stream function [-]
${}_1H_1$	Confluent hypergeometric function [-]
M	Magnetic parameter [-]
Nu	Nusselt number [-]
N_i	Heat source/sink factor [-]
N_r	Radiation factor [-]
Pr	Prandtl number [-]
q_r	Radiative heat flux $[Wm^{-2}]$
Q_0	Heat Source/sink factor [-]
Re	Reynolds number [-]
S	Mass suction/injection [-]
T	Temperature of the fluid $[K]$
T_w	Temperature of the surface $[K]$
T_∞	Ambient temperature $[K]$
u, v	x, y axis momentum components $[ms^{-1}]$

Greek symbols

α	Stretching/shrinking parameter [-]
β	Solution domain [-]
λ	Biviscosity Bingham fluid parameter [-]
ρ	Fluid density [kg m^{-3}]
μ	Viscosity of the fluid $[P\ s]$
σ	Electrical conductivity $[S/m]$
θ	Fluctuating temperature [-]
κ^*	Absorption coefficient [-]
ν	Kinematic viscosity $[m^2s^{-1}]$
η	Similarity variable [-]
σ^*	Stephen Boltzmann constant [-]
ψ	Stream function [-]
κ	Thermal conductivity [-]

Abbreviations

HNF	Hybrid nanofluid [-]
ODE	Ordinary differential equation [-]
PDE	Partial differential equation [-]

science. Ranga Babu *et al.* [10] and Ingham *et al.* [11] studied the analysis of hybrid nanofluids influence on transport processes in a porous medium. Maranna *et al.* [12] studied the impact of the Brinkman method in non-Newtonian fluid transfer caused by the porous sheet that was shrinking or stretching while simultaneously conducting heat transfer. Kasaeian [13] and Mishra *et al.* [14] studied the summary of the most recent advancements in nanofluid flow and thermal distribution in porous media on clean combustion in med of porous. hydrocarbon fuel combustion on the porous medium and the effect of core wettability on polymer adsorption and retention in the porous medium was explored by Howel *et al.* [15] and Broseta [16]. Jiang *et al.* [17] explored the concept of sintered porous plates with numerical modeling of fluid flow along with heat transfer. The viscoelastic fluid used by Sachhin *et al.* [18] to study the effect of magnetohydrodynamics caused by suction over a stretching sheet with a porous medium.

Being a fundamental feature of matter dependent on its temperature, thermal radiation is one of the three fundamental types of heat transport (conduction, convection, and radiation). Thermal radiation properties depend on the temperature of the source material. Astanina *et al.* [19] focussed on the heat source/sink effect over a porous medium with cooling the heat-generating element. Bingham fluid was used by Hamid *et al.* [20] to study the mass and thermal transpiration over an expansion/shrinking sheet. Thermal characteristics and improved heat transmission of a Bingham fluid through a porous media and analysis on Bingham fluid flow over a shrinking/stretching sheet for the heat and mass transfer studied by Khan [21,22]. Afterward, Liu *et al.* [23]

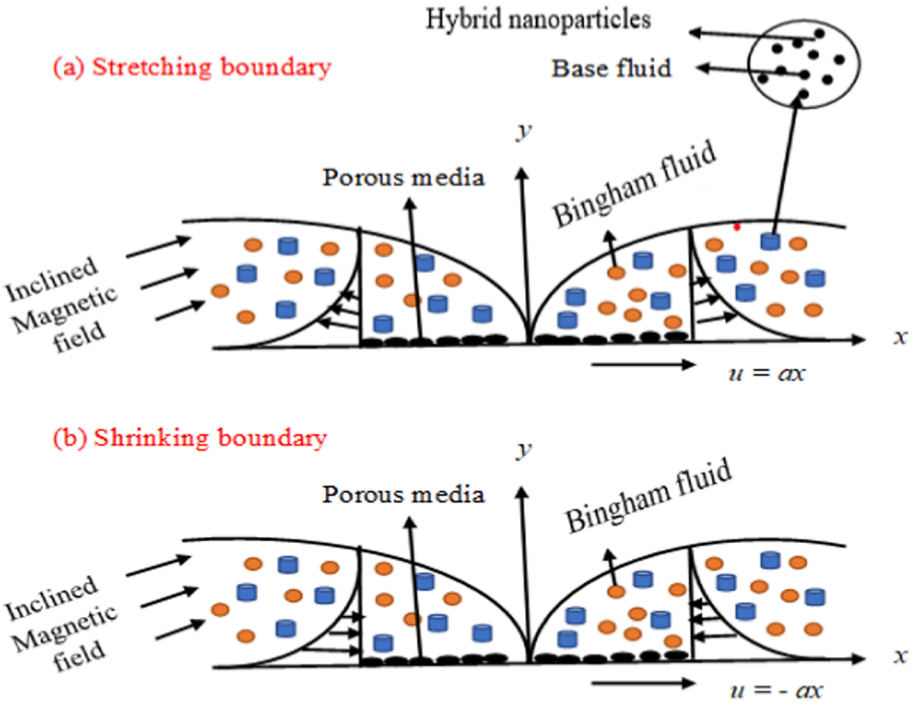

Fig. 1. Schematic diagram of the problem.

conducted research on hydromagnetic circulation across a stretching/shrinking sheet with heat and mass transfer. Chemical reactions and porous medium with the effect of both radiation and heat source/sink were studied by Mahabaleshwar *et al.* [24] same work extended by Mahesh *et al.* [25] explores the radiation effect on a porous sheet hybrid nanofluid flow under the MHD combine stress with viscous dissipation.

Effects of the Bingham model on a moving thin needle's hybrid nanofluid flow with a fractional model with heat and mass transfer were studied by Reddy [26] and Arif [27]. Kerosene oil and water base fluid were used by the Raja [28] to study the influence of MHD over the inclined surfaces. Plasma discharges have been studied by Manzoor [29] for the sterilization of infectious bacteria. Usman [30] explored the impact of a chemical reaction and activation energy over the fluid flow across the stretching surface. Eyring Powell nanofluid was used by Ijaz [31] to study the swimming characteristics of gyrotactic microorganisms over the surface of the Riga plate. Afterward, Mahabaleshwar et al. [32] studied the homogeneous–heterogeneous (H–H) reactions and Hall current with the effect of MHD (magnetohydrodynamics). Nonlinear mixed convection in the dissipative convective flow of micropolar fluid toward a stretched surface was explored by Khan et al. [33]. Some important results in the flow of viscous and non-Newtonian materials are presented in Refs. [34–39], Ramesh et al,[40] studied the flow of Carreau nanofluids through the micro-channel with the effects of electro-osmosis, Joule heating, and chemical reactions. A stretchable disk was used by [41] to study the hydromagnetic flow of magnetite-water nanofluid by using the Buongiorno model.

Inspired by the aforementioned discoveries and applications, the present article studies the impact of radiation and inclined magnetic field on the biviscosity Bingham hybrid nanofluid flow across permeable stretching/shrinking surfaces. It is noted that there is a lack of study on Bingham liquids in the circumstances of MHD and radiation with permeable media. The novelty of the present problem is to study the influence of magnetic field and radiation over bi-viscosity Bingham hybrid nanofluid flow. Similarity transformation is used to reduce the governing equations of the problem into a system of nonlinear ordinary differential equations, and current research illustrates that the temperature and momentum equation solutions by the analytical method to obtain the exact solution and express the solution domain in terms of hypergeometric function, and discussed results of the porous medium, mass transpiration, volume fraction, skin friction and Nusselt number from graphs and tables, the results and main contribution of the current study can be applicable in the development of efficient fuel cells, polymer industry with respect to stretching/shrinking sheets.

2. Mathematical formulation

Consider the two-dimensional laminar flow of Bingham hybrid nanofluid over a porous stretching/shrinking sheet. Let the velocity of the sheet $U_w = ax$ where $a > 0$. A fluid flow sheet is considered along the x-axis and the y − axis is perpendicular to it, as shown in Fig. 1. Flow is being held to $y > 0$, and the fluid's motion is assumed to be aided by an inclined magnetic field.

The rheological equation of biviscosity Bingham fluid is given as follows [26].

$$\tau_{ij} = \begin{cases} 2(\mu_B + p_y/\sqrt{2\pi})e_{ij}, & \pi > \pi_c, \\ 2(\mu_B + p_y/\sqrt{2\pi})e_{ij}, & \pi < \pi_c, \end{cases} \tag{1}$$

where deformation rate product is defined as π, the product value of biviscosity Bingham model is denoted as π_c, P_y defined as yields stress of the fluid model, μ_B denoted as the viscosity of plastic deformation.

Governing equations of continuity, momentum, and temperature are followed as [20, 21, and 22].

$$\frac{\partial u}{\partial x} + \frac{\partial v}{\partial y} = 0, \tag{2}$$

$$u\frac{\partial u}{\partial x} + v\frac{\partial u}{\partial y} = \frac{\mu_{hnf}}{\rho_{hnf}}\left(1 + \frac{1}{\lambda}\right)\frac{\partial^2 u}{\partial y^2} - \frac{\sigma_{hnf}}{\rho_{hnf}}B_0^2 \mathrm{Sin}^2(\tau)u - \frac{\nu_{hnf}}{k}u, \tag{3}$$

$$u\frac{\partial T}{\partial x} + v\frac{\partial T}{\partial y} = \frac{\kappa_{hnf}}{(\rho C_p)_{hnf}}\frac{\partial^2 T}{\partial y^2} - \frac{1}{(\rho C_p)_{hnf}}\frac{\partial q_r}{\partial y} + \frac{Q_0(T - T_\infty)}{(\rho C_p)_{hnf}}, \tag{4}$$

Boundary Conditions are given by [20].

$$u = ax,\ v = v_w\ -k\frac{\partial T}{\partial y} = h(T_w - T),\ as\ \ y \to 0,$$

$$u = 0, T = T_\infty, at y \to \infty, \tag{5}$$

where u is the component of velocity along x and v is the component of velocity *y-axis* respectively, λ is the biviscosity Bingham fluid parameter, ν is the dynamic viscosity, $B_0^2\mathrm{Sin}^2(\tau)$ denotes the inclined magnetic field, ρ denotes density, κ is the thermal conductivity, σ is the electrical conductivity, and T is the temperature. Introducing the transformed similarity variables into the system of PDEs [23]:

$$u = axf_\eta(\eta), v = -\sqrt{a\nu}f(\eta), \eta = y\sqrt{\frac{a}{\nu}}, \theta(\eta) = \frac{T - T_\infty}{T_w - T_\infty}. \tag{6}$$

The radiation heat flux was q_r formulated using Rosseland's approach [24].

$q_r = -\frac{4\sigma^*}{3\kappa^*}\frac{\partial T^4}{\partial y}$ (7) where κ^* is the absorption parameter and σ^* is the Stephen Boltzmann constant, we use Rosseland's approach, to elaborate T^4 with Taylor series expansion, and ignore the high order elements for obtaining.

$$T^4 \cong 4T_\infty^3 T - 3T_\infty^4 \tag{8}$$

the radiation effect in equation number (4) is differentiated and produced in the form of

$$\frac{\partial q_r}{\partial y} = -\frac{16\sigma^*}{3\kappa^*}\frac{\partial^2 T}{\partial y^2} \tag{9}$$

By using above Eq. (8) and (9) substituted in Eq. (4) we get

$$u\frac{\partial T}{\partial x} + v\frac{\partial T}{\partial y} = \left(\frac{\kappa_{hnf}}{(\rho C_p)_{hnf}} - \frac{1}{(\rho C_p)_{hnf}}\frac{16\sigma^*}{3\kappa^*}\right)\frac{\partial^2 T}{\partial y^2} + \frac{Q_0(T - T_\infty)}{(\rho C_p)_{hnf}} \tag{10}$$

By using similarity variables Eq. (6), calculated the Eq. (3) and (10) we get

$$\left(1 + \frac{1}{\lambda}\right)f_{\eta\eta\eta}(\eta) - \frac{A_2}{A_1}[f_\eta(\eta)]^2 + \frac{A_2}{A_1}f_{\eta\eta}(\eta)f(\eta) - \left(\frac{A_3}{A_1}MSin^2(\tau) + Da^{-1}\right)f_\eta(\eta) = 0 \tag{11}$$

$$(A_4 + N_r)\theta_{\eta\eta}(\eta) + A_5 Pr\theta_\eta(\eta)f(\eta) + N_i Pr\theta(\eta) = 0 \tag{12}$$

where$M = \frac{\sigma_f B_0^2}{\rho_f a}$ denotes the magnetic field parameter,$Da^{-1} = \frac{\nu_f}{ka}$ denotes the inverse Darcy number.Pr denotes the Prandtl number,$N_i = \frac{Q_0}{\rho C_f}$ denotes the Heat source/sink,$A_1 = \frac{\mu_{hnf}}{\mu_f}, A_2 = \frac{\rho_{hnf}}{\rho_f}, A_3 = \frac{\sigma_{hnf}}{\sigma_f}, A_4 = \frac{\kappa_{hnf}}{\kappa_f}, A_5 = \frac{(\rho C_p)_{hnf}}{(\rho C_p)_f}$.are constants.

Modified boundary conditions are as follows:

$$f(\eta) = S, f_\eta(\eta) = \alpha, \theta_\eta(\eta) = -Bi(1 - \theta(\eta)), as \eta \to 0,$$

$$f_\eta(\eta) = 0, \theta(\eta) = 0, at \eta \to \infty \tag{13}$$

Following Mahesh *et al.* [25]. The heat capacity, density, thermal conductivity, and viscosity of hybrid nanofluid were obtained as.

$$\left.\begin{aligned}
\frac{\rho_{hnf}}{\rho_f} &= (1-\phi_2)\left(1-\phi_1+\phi_1\left(\frac{\rho_{s_1}}{\rho_f}\right)\right)+\phi_2\left(\frac{\rho_{s_2}}{\rho_f}\right)\\
\frac{\sigma_{hnf}}{\sigma_f} &= \frac{\sigma_{s_2}+2\sigma_{bf}+2\phi_2(\sigma_{s_2}-\sigma_f)}{\sigma_{s_2}+2\sigma_{bf}-\phi_2(\sigma_{s_2}-\sigma_f)}\\
&where\\
\frac{\sigma_{bf}}{\sigma_f} &= \frac{\sigma_{s_1}+2\sigma_f+2\phi_1(\sigma_{s_1}-\sigma_f)}{\sigma_{s_1}+2\sigma_f-\phi_1(\sigma_{s_1}-\sigma_f)}\\
\frac{\mu_{hnf}}{\mu_f} &= \frac{1}{(1-\phi_1)^{2.5}(1-\phi_2)^{2.5}}\\
\frac{(\rho C_p)_{hnf}}{(\rho C_p)_f} &= (1-\phi_2)\left(1-\phi_1+\phi_1\left(\frac{(\rho C_P)_{s_1}}{(\rho C_P)_f}\right)\right)+\phi_2\left(\frac{(\rho C_P)_{s_2}}{(\rho C_P)_f}\right)\\
\frac{\kappa_{hnf}}{\kappa_f} &= \frac{\kappa_{s_2}+2\kappa_{bf}+2\phi_2(\kappa_{s_2}-\kappa_f)}{\kappa_{s_2}+2\kappa_{bf}-\phi_2(\kappa_{s_2}-\kappa_f)}\\
&where\\
\frac{\kappa_{bf}}{\kappa_f} &= \frac{\kappa_{s_1}+2\kappa_f+2\phi_1(\kappa_{s_1}-\kappa_f)}{\kappa_{s_1}+2\kappa_f-\phi_1(\kappa_{s_1}-\kappa_f)}
\end{aligned}\right\} \quad (14)$$

in which $\mu_f, \rho_f, (C_p)_f, \kappa_f$, and σ_f are forceful dynamic viscosity, density, heat capability, thermal conductivity, and electrical conductivity of the base fluid. ρ_{S_1}, ρ_{S_2}, $(C_p)_{S_1}, (C_p)_{S_2}$, $\kappa_{S_1}, \kappa_{S_2}$, $\sigma_{S_1}, \sigma_{S_2}$ are the densities, capacities, heat conductivities and electrical conductivities of the used nanoparticles. ϕ_1, ϕ_2 are the solid volume fraction of the first, second nanoparticles.

3. Analytical solution for momentum equation

Here we explain the procedure of the exact solution method. We must get the analytic solution to the equation (11) along with the boundary conditions (13). We obtain the exact solution to equation (11) by the below procedure [20].

$$f(\eta) = S+\frac{\alpha}{\beta}(1-e^{-\beta\eta}) \quad (15)$$

Differentiate the above equation we get.

$$f_\eta(\eta) = \alpha e^{-\beta\eta}, f_{\eta\eta}(\eta) = -\alpha\beta e^{-\beta\eta}, f_{\eta\eta\eta}(\eta) = \alpha\beta^2 e^{-\beta\eta}. \quad (16)$$

Substitute equations (16) & (17) in (11), we get a quadratic equation in terms of β.

$$\left(1+\frac{1}{\lambda}\right)A_1\beta^2 - A_2S\beta - A_3M\mathrm{Sin}^2(\tau) - A_1Da^{-1} - A_2\alpha = 0 \quad (17)$$

which gives two roots for the above equation as follows

$$\beta_1 = \frac{A_2S+\sqrt{A_2^2S^2-4A_1\left(-A_1Da^{-1}-A_3M\mathrm{Sin}^2(\tau)-A_2\alpha\right)\left(1+\frac{1}{\lambda}\right)}}{2\left(A_1+\frac{A_1}{\lambda}\right)}$$

and

$$\beta_2 = \frac{A_2S-\sqrt{A_2^2S^2-4A_1\left(-A_1Da^{-1}-A_3M\mathrm{Sin}^2(\tau)-A_2\alpha\right)\left(1+\frac{1}{\lambda}\right)}}{2\left(A_1+\frac{A_1}{\lambda}\right)}$$

Further, we acquire the results for our present work by the above-mentioned different roots.

4. The skin friction is formulated as follows

Skin friction can be calculated as follows.

Skin friction $\mathrm{Re}^{1/2}C_f = A_1\left(1+\frac{1}{\lambda}\right)f_{\eta\eta}(\eta)$,

$$Nu\mathrm{Re}^{1/2} = (A_4+Nr)\theta_\eta(\eta) \quad (18)$$

where$\mathrm{Re} = \frac{U_w x}{\nu_f}$. Represents local Reynolds number.

5. Analytical solution for temperature equation

We must get an analytical solution for equation (12), So we introduce a new variable using this in equation (12) and expressing boundary conditions (13), which gives the below result

$$t\frac{d^2\theta}{d\theta^2}+(1-m+nt)\frac{d\theta}{dt}+L\theta = 0 \quad (19)$$

where

$$m = \frac{A_5S\mathrm{Pr}}{(A_4+Nr)\beta}+\frac{A_5\mathrm{Pr}\alpha}{\beta^2(A_4+Nr)}, n = \frac{A_5\mathrm{Pr}\alpha}{(A_4+Nr)}, L = \frac{Ni\mathrm{Pr}}{\beta^2(A_4+Nr)}.$$

Additional boundary conditions are [20,35,36].

$$\frac{\mathrm{Pr}}{\beta}\frac{d\theta}{dt}\left(\frac{\mathrm{Pr}}{\beta^2}\right) = Bi\left(1-\theta\left(\frac{\mathrm{Pr}}{\beta^2}\right)\right), and\theta(0) = 0, \quad (20)$$

to solve equation (19) we have the power series solution $\theta(t) = \sum_{r=0}^{\infty}a_r t^{r+k}$ by applying the Frobenius method to get the unique characteristics and solution as the analytical solution obtain

$$\theta(t) = \frac{\frac{Bi}{A_4}\left(e^{(-\beta\eta)}\right)^{\frac{k_1+k_2}{2}}H\left[\frac{k_1+k_2}{2}, k_2+1, -npe^{(-\beta\eta)}\right]}{\left(\beta^{\frac{k_1+k_2}{2}}\right)H\left[\frac{k_1+k_2}{2}, k_2+1, -np\right] - \frac{np}{k_2+1}H\left[\frac{k_1+k_2}{2}+1, k_2+2, -np\right] + \frac{L}{A_4}H\left[\frac{k_1+k_2}{2}, k_2+1, -np\right]} \quad (21)$$

where

$$L = \frac{\mathrm{Pr}Ni}{\beta^2(A_4+Nr)}, k_1 = m, k_2 = \sqrt{m^2-4L}, m = \frac{A_5S\mathrm{Pr}}{(A_4+Nr)\beta}+\frac{A_5\mathrm{Pr}d}{\beta^2(A_4+Nr)}, n = \frac{A_5\mathrm{Pr}d}{(A_4+Nr)},$$

Table 1
Thermophysical properties of nanoparticles [26,27]:

Properties	$C_2H_6O_2$	MoS_2	GO
σ	1.07×10^{-4}	2.09×10^{-4}	3.2×10^{-4}
$\rho(kgm^{-3})$	2430	5.06×10^{3}	1800
$C_p(JkgK^{-1})$	1115	397.21	717
$k(WmK^{-1})$	0.253	904.4	5000

in this portion, calculate the hypergeometric function as a problem-solving method that gives a solution.

6. Nusselt number coefficient calculated as below

Nusselt number can be calculated as follows

$$C_f = \frac{\tau_w}{\rho_f} = \frac{\mu_{hnf}}{\rho_f U_w^2}\frac{\partial u}{\partial y}\bigg|_{y=o} \tag{22}$$

Nusselt number $Nu = \frac{xq_w}{\kappa_{hnf}(T_w - T_\infty)}$,where

$$q_w = -\left(\left(\frac{16\sigma^* T_\infty^3}{3K^*} + \kappa_{hnf}\right)\right)\left(\frac{\partial T}{\partial y}\right)_{y=0} \tag{23}$$

6.1. Validation

The research reveals the effect of radiation and inclined magnetic field on the biviscosity Bingham hybrid nanofluid flow on the permeable stretching/shrinking surface with mass transpiration. The absence of Solid volume fraction ($\phi = 0$), magnetic field ($M = 0$), and porous

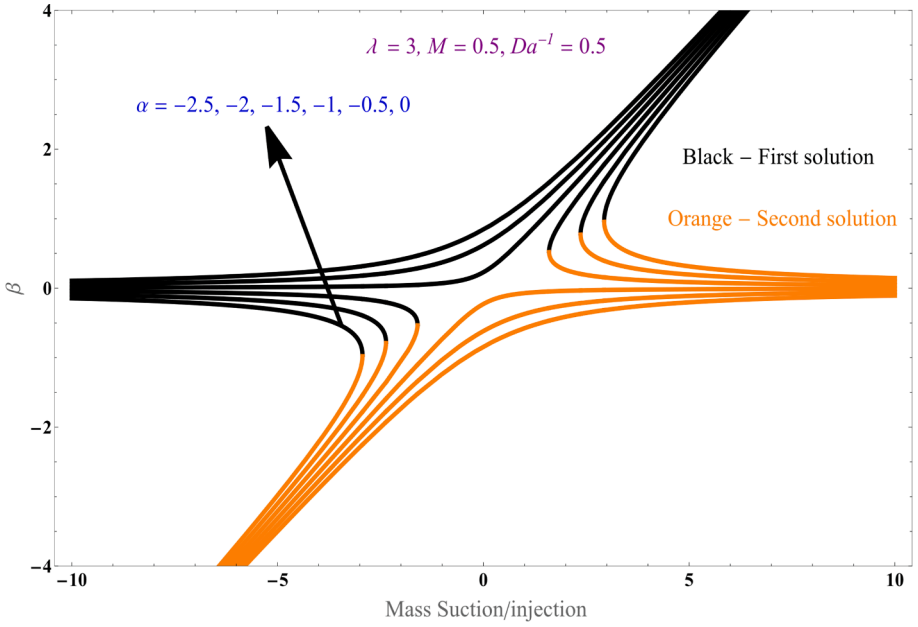

Fig. 2. Graph of Solution domain β as a function of mass injection/suction parameter S.

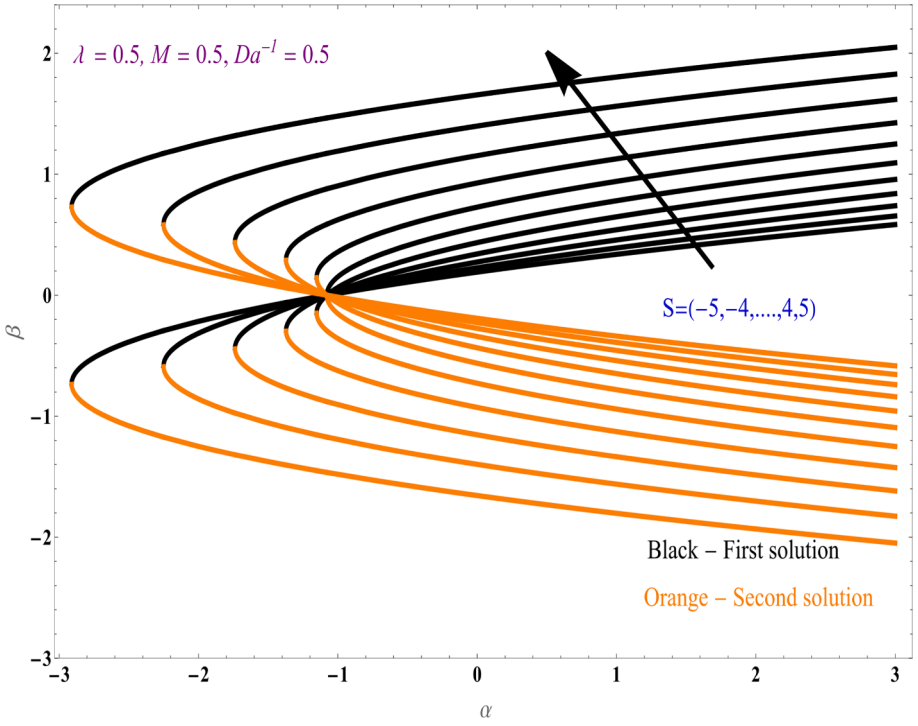

Fig. 3. Graph of solution domain β as a function of α parameter.

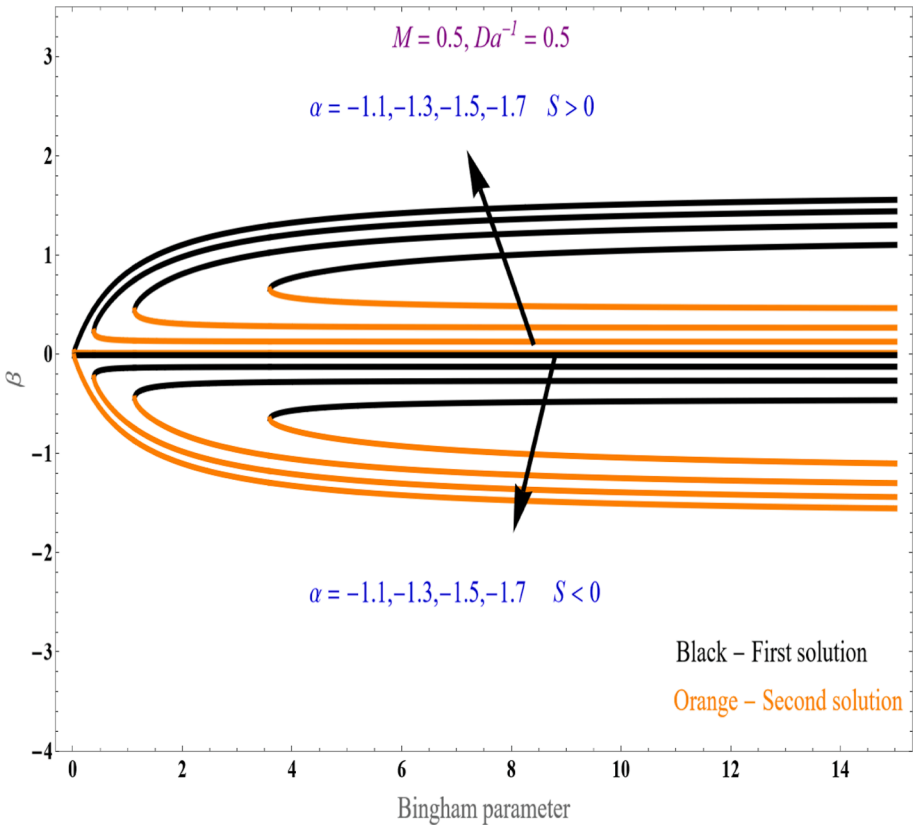

Fig. 4. Graph of solution domain with biviscosity Bingham parameter λ.

media ($Da^{-1} = 0$) leads to the results of Hamid *et al.* [20] (2019). The absence of a heat source/sink ($Q_o = 0$), magnetic field ($M = 0$), and porous media ($Da^{-1} = 0$) leads to the results of Mahabaleshwar *et al.* [32] (2022). The presence of a hybrid nanofluid, the absence of a porous medium ($Da^{-1} = 0$), and the inclined angle ($\tau \to 90^{\cdot}$), lead to the results of Khan *et al.* [33] (2022). In the presence of a hybrid nanofluid, the absence of heat source/sink ($Q_o = 0$), inclined angle ($\tau \to 90^{\cdot}$), and biviscosity Bingham parameter, leads to results of Mahesh *et al.* [34] (2023).

The next part, discusses the results and discussion of the current study.

7. Results and discussion

The present work focuses on the inclined magnetic field over a biviscosity Bingham fluid along with heat transfer across both stretching

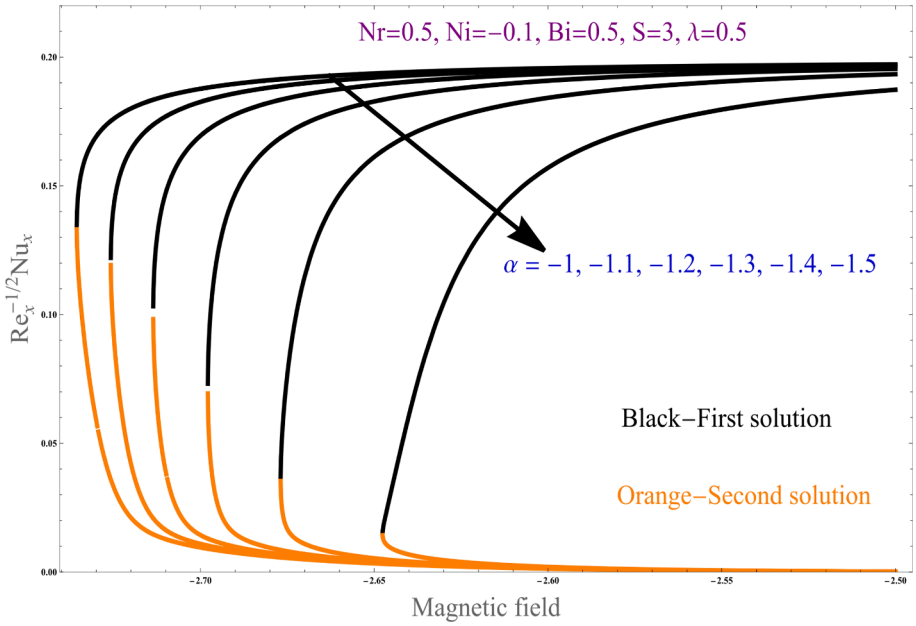

Fig. 5. Graph of variations of heat transfer coefficient with magnetic field M.

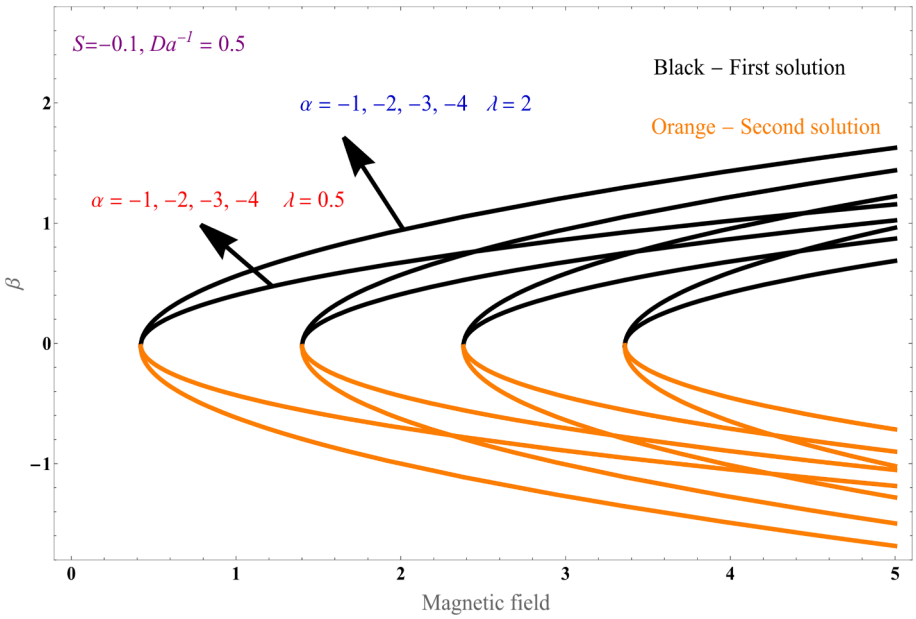

Fig. 6. Graph of solution domain with magnetic field M.

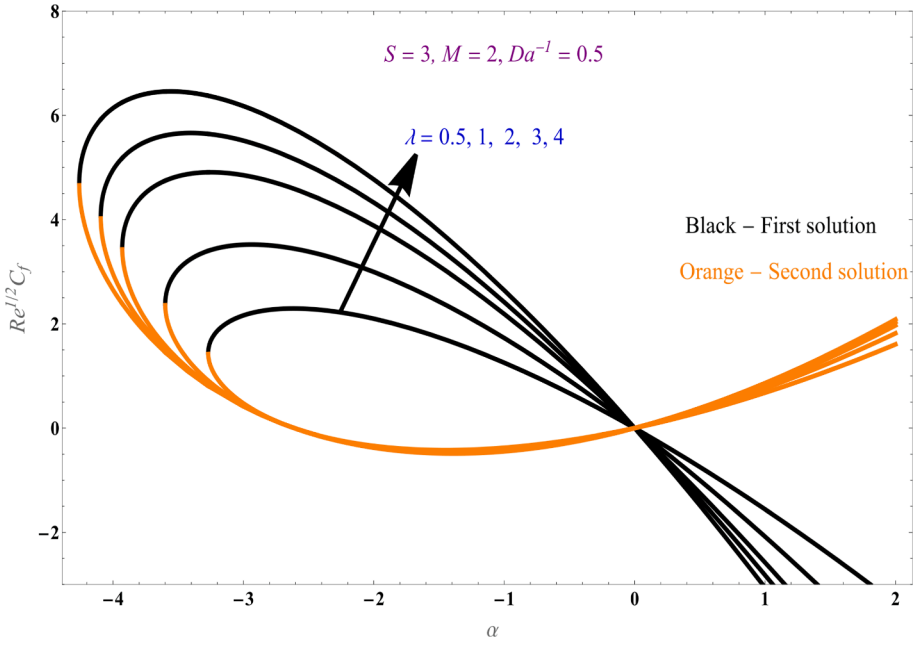

Fig. 7. Graph of skin friction with α parameter.

and shrinking boundary, the impact of radiation heat source/sink is also examined. While inserting the similarity transformation to the governing equation to obtain in terms of simplified non-linear ODEs. Examining the graphs of higher and lower solution branches' responses on the hybrid nanofluid was the closest form of exact solutions for our problem. Showed the influences of physical characteristics like inclined magnetic field, thermal radiation factor, temperature, mass suction/injection, heat source and sink, Biot number, and Darcy number with the graphs. Setting the numerical value of the Prandtl number Pr is 125 for Ethylene glycol, and the range of parameters taken as $-5\leqslant\alpha\leqslant5$, $-5\leqslant S\leqslant5$, $0.1\leqslant\lambda\leqslant4$, $0.1\leqslant M\leqslant4$, $1\leqslant Bi\leqslant3$, $0.5\leqslant Da^{-1}\leqslant4$, $-0.5\leqslant Ni\leqslant0.5$, $0.1\leqslant Nr\leqslant2$, $0.1\leqslant\phi<3$, thermos physical properties given in Table 1.

Fig. 2, displays the plots of the inclination of the solution domain β with the increasing values of the parameter and as a function of mass suction/injection parameter, while remaining physical parameters like biviscosity Bingham fluid parameter, inclined magnetic field, inverse Darcy number kept fixed, in the higher branch of the solution increase in the α parameter generates the rising in β. For the second branch solution, the streamline shows a decreasing nature. The negative profile β also shows in the lower branch of the solution.

Fig. 3, displays the plots of the inclination of the solution domain β with the function α parameter, with varying the mass injection/suction parameter, while remaining parameters like inclined magnetic field, biviscosity Bingham fluid parameter and Da^{-1} kept fixed, in the upper branch biviscosity Bingham fluid parameter increases as suction/injection parameter increases. And reverse phenomena exhibited for streamlined profile observed in the second branch solution. It is observed that $\beta=0$ is a critical point to obtain both higher and lower

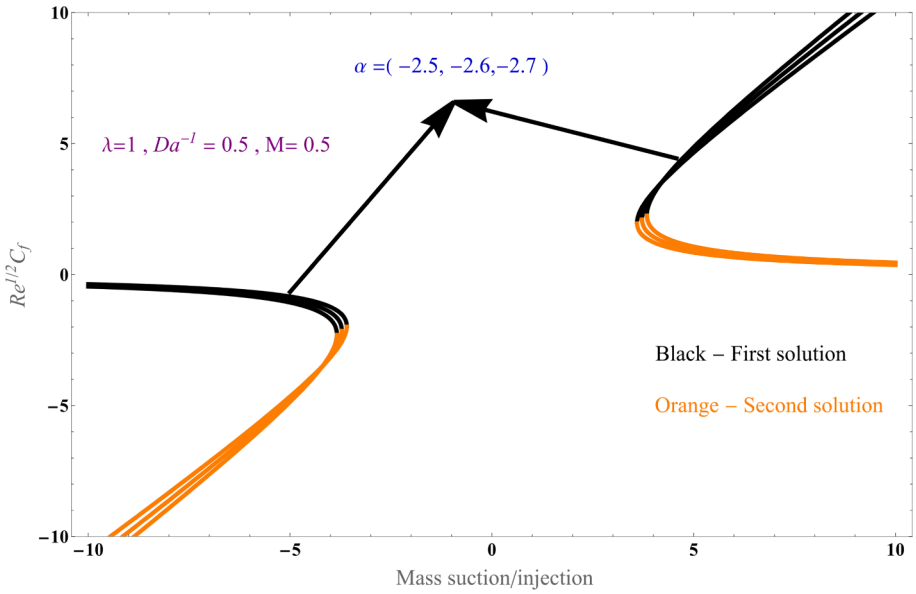

Fig. 8. Graph of variations of skin friction with S.

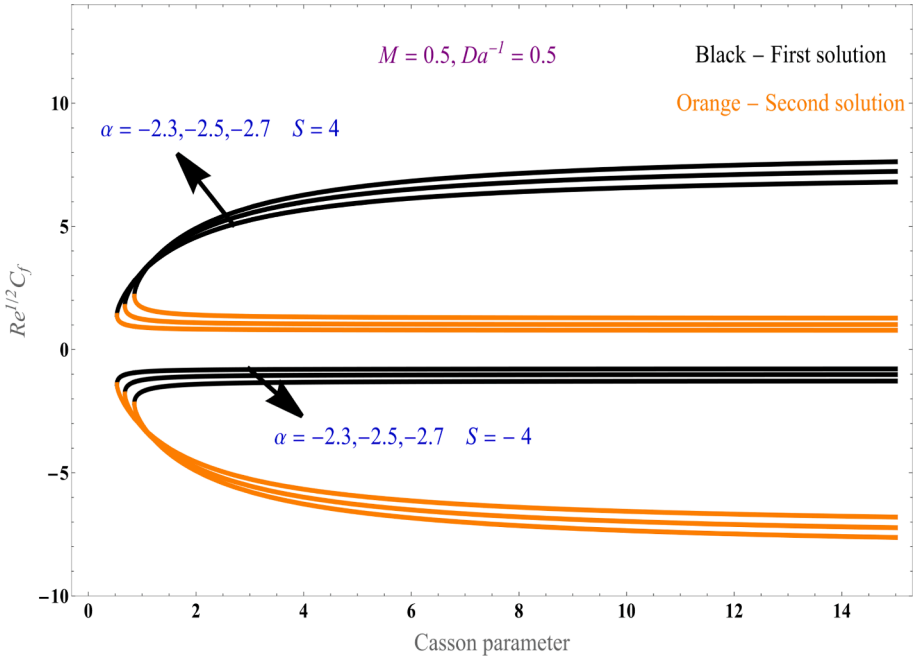

Fig. 9. Graph of skin friction with biviscosity Bingham fluid parameter λ.

branches with different values of S in biviscosity Bingham fluid.

Fig. 4 displays the plot β as a function of the biviscosity Bingham parameter, taking different values while the magnetic field and inverse Darcy number are kept constant. taken both positive and negative values of mass suction/injection parameter, both higher and lower branch increases for the positive value of mass suction/injection values, but for negative value both upper and lower branch decreases and shows reverse in nature for the biviscosity Bingham fluid flow across the shrinking sheet.

Fig. 5, represents the graph of the heat transfer coefficient as a function of the magnetic field, while keeping all other parameters constant, as we decrease the value of the α parameter the higher branch solution shows an increase in nature while the second branch solution shows a decrease in nature. The magnetic field of the biviscosity Bingham fluid across the surface increases the Nusselt coefficient for both higher and lower branch solutions.

Fig. 6 displays the influence of the magnetic field with the presence of negative mass suction/injection parameter of the biviscosity Bingham fluid, inverse Darcy number taken as constant, for increasing values of dual branch solutions, we are observing that increasing in the Bingham parameter the higher branch dramatically increases and for the second branch solution β is declining.

Fig. 7 portrays the graph of variations of Skin friction α, with the presence of positive mass suction/injection parameter of biviscosity Bingham fluid across the sheet, and taken magnetic field and inverse Darcy number kept constant, while we increase the biviscosity Bingham fluid parameter the upper branch shows an increase in nature and lower branch solution exhibits declining nature, and magnetic field also affects over the dual solution nature of skin friction factor.

Fig. 8, displays the plots for variations of skin friction as a function of

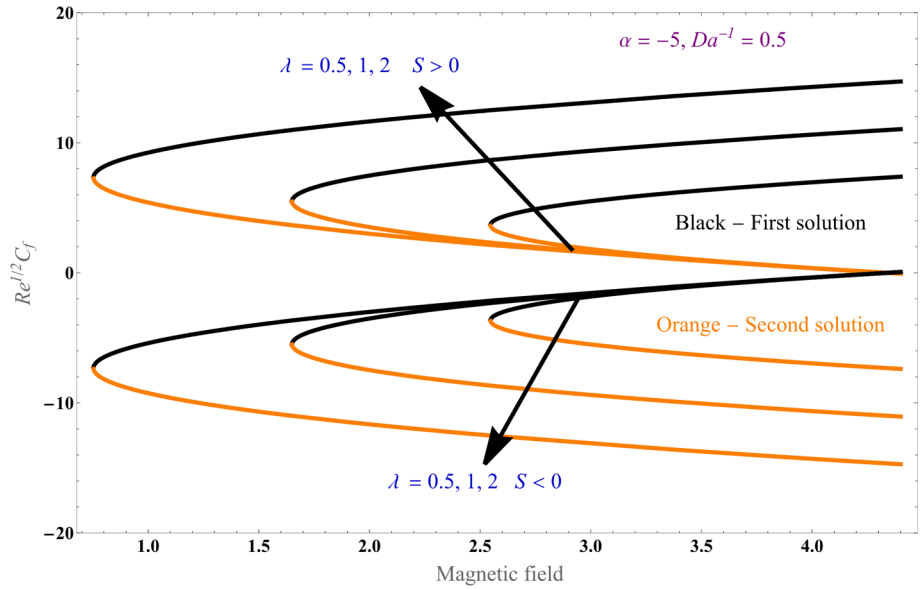

Fig. 10. Graph of skin friction as a function of magnetic field *M*.

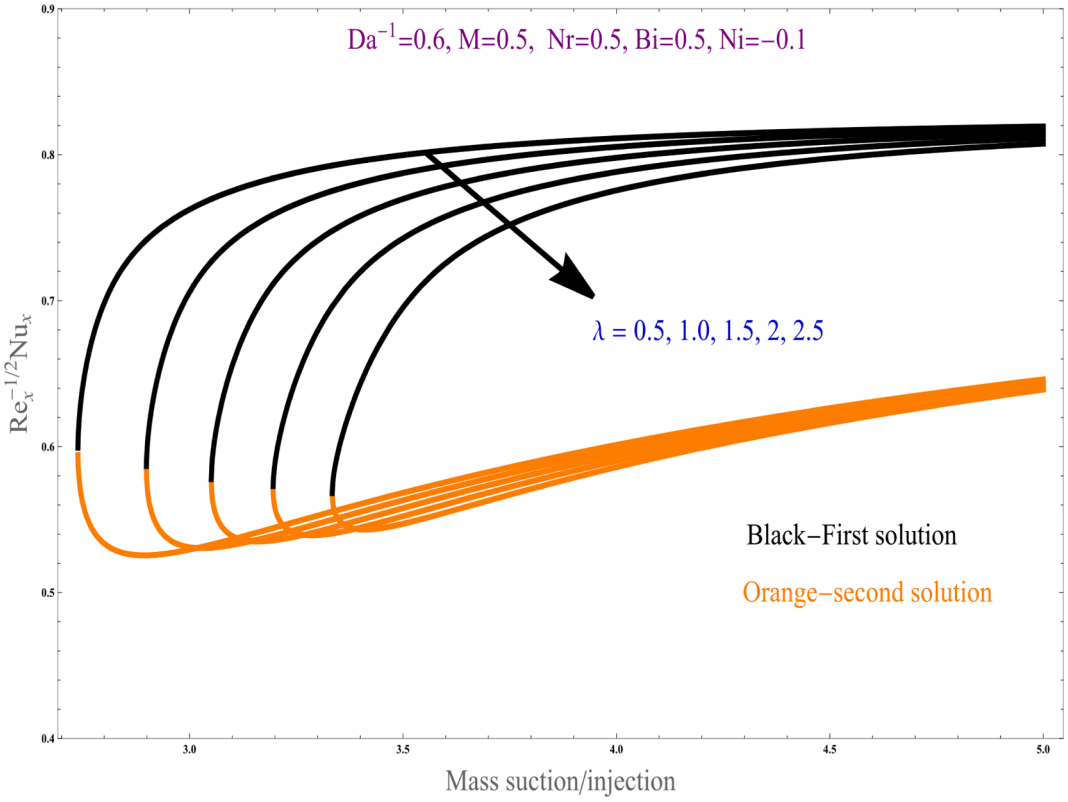

Fig. 11. Graph of Nusselt number with *S* by varying biviscosity Bingham parameter λ.

S, taking inverse Darcy number and Hartman number, biviscosity Bingham fluid parameter as constant, and varies α parameter, with the presence of biviscosity Bingham fluid flow across the sheet, while rising the α value the coefficient of skin friction gets weaker, and the reverse phenomena exhibits for stretching boundary, for the positive value of mass suction/injection the coefficient of skin friction found larger than the negative value of mass suction/injection.

Fig. 9 displays the tendency of skin friction to co-efficient with the biviscosity Bingham fluid parameter, while taking the inverse Darcy number and Hartman number as constant, we observe that by raising the α parameter both upper and second branch solutions show decreasing nature for mass injection value, and both higher and second branch solutions increase for mass suction value, and we noticed that dual solution of skin friction coefficient gets higher with rising the mass suction of Bingham fluid flow over the sheet.

Fig. 10 displays the impact of Skin friction over the magnetic field, taking the negative α parameter and inverse Darcy number kept constant, by raising the biviscosity Bingham parameter both the higher and lower branch gets increasing for the mass injection, and both upper and lower branches show decreasing nature for the mass suction parameter.

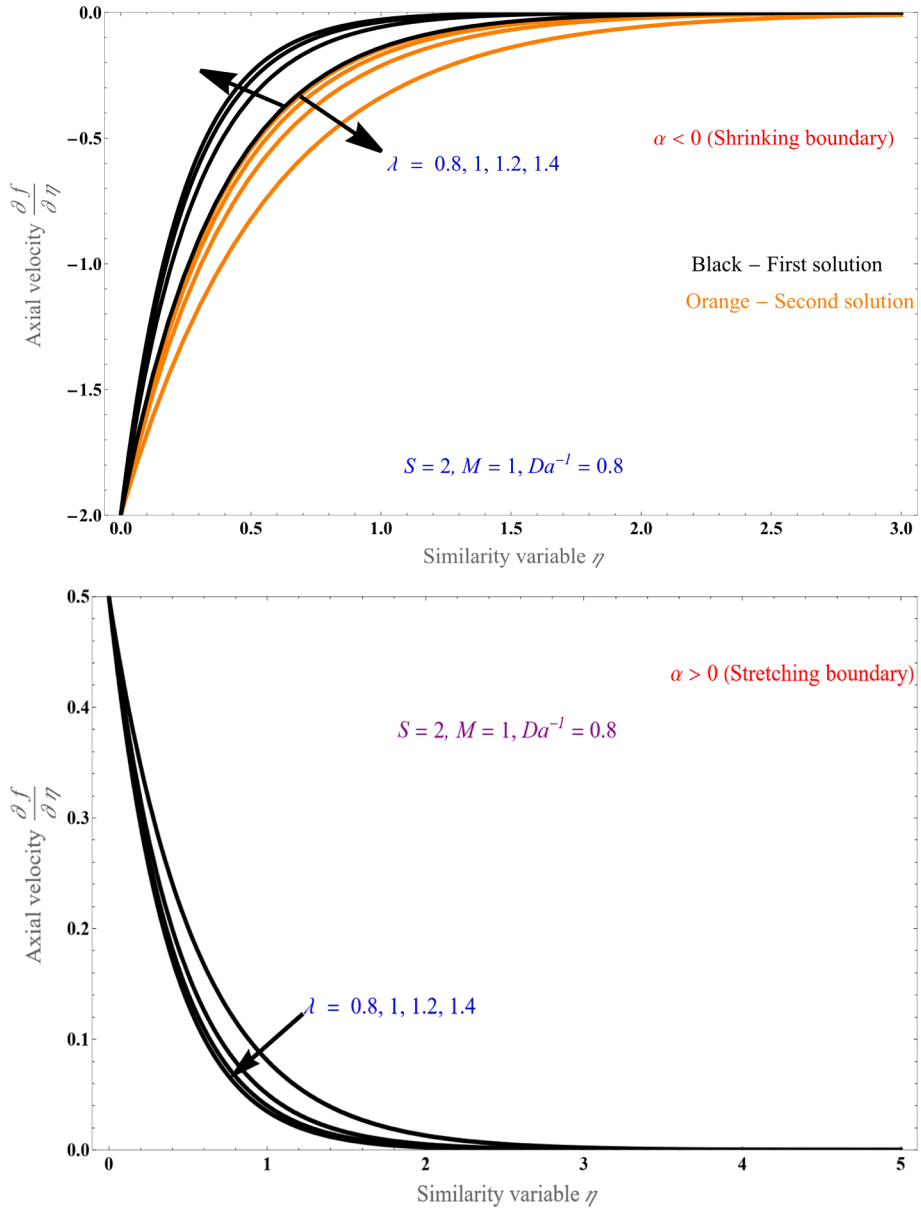

Fig. 12. (a): Graph of velocity with the similarity variable η. (b): Graph of velocity with variation of λ.

Fig. 11, represents the graph of the Nusselt coefficient with mass suction/injection, while keeping all other parameters constant, the average Nusselt increases with increasing Bingham fluid parameter. As we increase the value of the biviscosity Bingham parameter the higher branch solution shows an increase in nature while the lower branch solution shows a decrease in nature. Mass absorption/generation of the Bingham fluid across the surface increases the heat transfer coefficient for both higher and second-branch solutions.

Fig. 12 (a) &Fig. 12 (b) represent the graphs of the velocity profile with the similarity variable. The Bingham parameter is the characteristic material parameter to describe the measure of the Bingham fluid and rising in the Bingham parameter decreases the velocity and momentum boundary layer thickness becomes thinner, in the first graph shrinking boundary exhibits the dual solution showing the increasing biviscosity Bingham parameter increases the higher branch solution but the lower branch solution shows the decreasing nature. The second graph for stretching boundary exhibits the unique solution and while raising the biviscosity Bingham parameter the first branch solution decreases. Bingham parameter has physical applications in paleo magnetic studies, material science, and probability theory.

Fig. 13 (a) and Fig. 13 (b) represent the graphs of the velocity profile with the similarity variable, the magnetic field encourages the resistive Lorentz force, which is present in an electrically conducting fluid, this force results in resistance to the fluid particle's momentum, which decays the fluid's velocity for the stretching surface. Physically, an upsurge in the magnetic parameter makes it harder for the fluid to move, rise in the magnetic parameter decreases the momentum boundary layer, the first graph shrinking boundary exhibits the dual solution showing the increasing magnetic field increases the higher branch solution but a lower branch solution shows the decreasing nature. The second graph for stretching boundary exhibits the unique solution and while raising the magnetic field the first branch solution shows a decrease in nature. Magnetic field parameter has physical applications in both electric motors and generators and mass spectrometry, magnetic resonance imaging (MRI), magnetic levitation, compasses, etc.

Fig. 14 (a)&Fig. 14 (b) represents the graphs of the velocity profile with the similarity variable, while keeping the biviscosity Bingham fluid parameter, magnetic field, and inverse Darcy number constant, mass

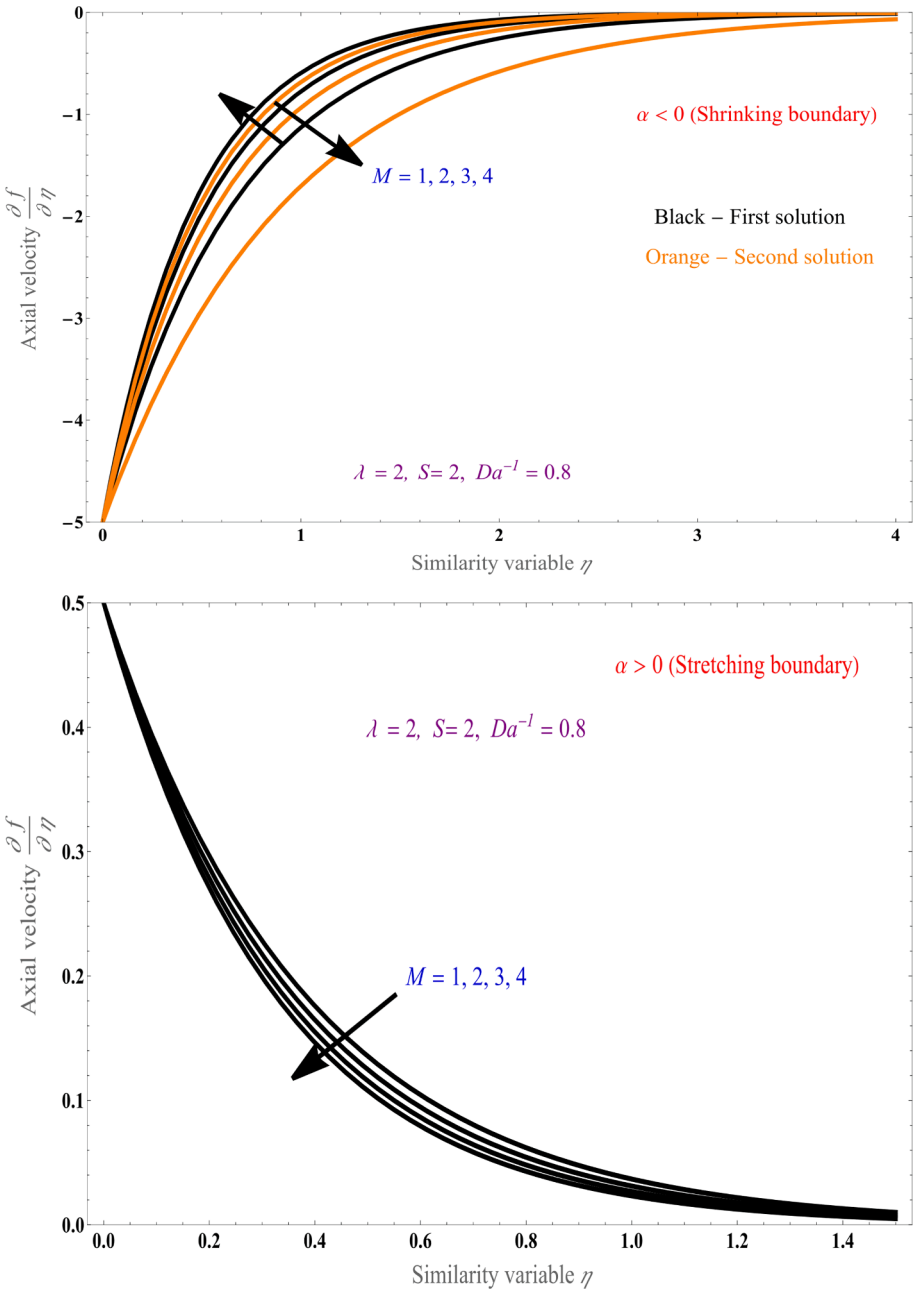

Fig. 13. (a): Graph of Velocity with the similarity variable variation of Magnetic field *M*. (b): Graph of velocity with variation of magnetic field *M*.

suction/injection refers to the process of introducing or removing fluid from a system through boundary surfaces, this process can significantly change the flow field and is applied to minimize energy losses due to surface drag, the first graph shrinking boundary exhibits the dual solution shows the increasing of mass suction/injection parameter increases the higher branch solution but lower branch solution shows the decreasing nature. The second graph for the stretching boundary exhibits the unique solution and while raising the mass suction/injection parameter the first branch solution shows a decrease in nature. Mass suction/injection plays a critical function in boundary layer control, particularly in engineering, aerodynamics, and space research, the suction/injection effect is significant in the boundary flow and is applied to minimize the energy losses due to the surface drag this effect is also applied to construct biological and mechanical suction devices.

Fig. 15 (a) & Fig. 15 (b) represent the graphs of the temperature profile with the similarity variable, while keeping the biviscosity Bingham fluid parameter, magnetic field, and inverse Darcy number constant, taking heat sink parameter and magnetic field as constant, the first graph shrinking boundary exhibits the dual solution shows the increasing of Biot number parameter increases the higher branch solution and lower branch solution. The second graph for stretching boundary exhibits the unique solution and while raising the Biot number parameter the first branch solution shows an increase in nature. Biot number is the ratio of the thermal resistance for conduction inside the body to the resistance for convection at the surface of the body due to these effects increase in the biot number increases the boundary layer thickness and temperature distribution. The biot number parameter shows the increasing nature of both stretching and shrinking boundary surfaces. Biot number is a useful temperature-controlling tool for analyzing heat transfer problems, particularly those involving transient heat conduction and fin heat transfer calculations, and also Biot number is used to estimate the controlling mechanisms employed for heat or mass transfer during the drying process.

Fig. 16 (a) &Fig. 16 (b) represent the graphs of the velocity profile

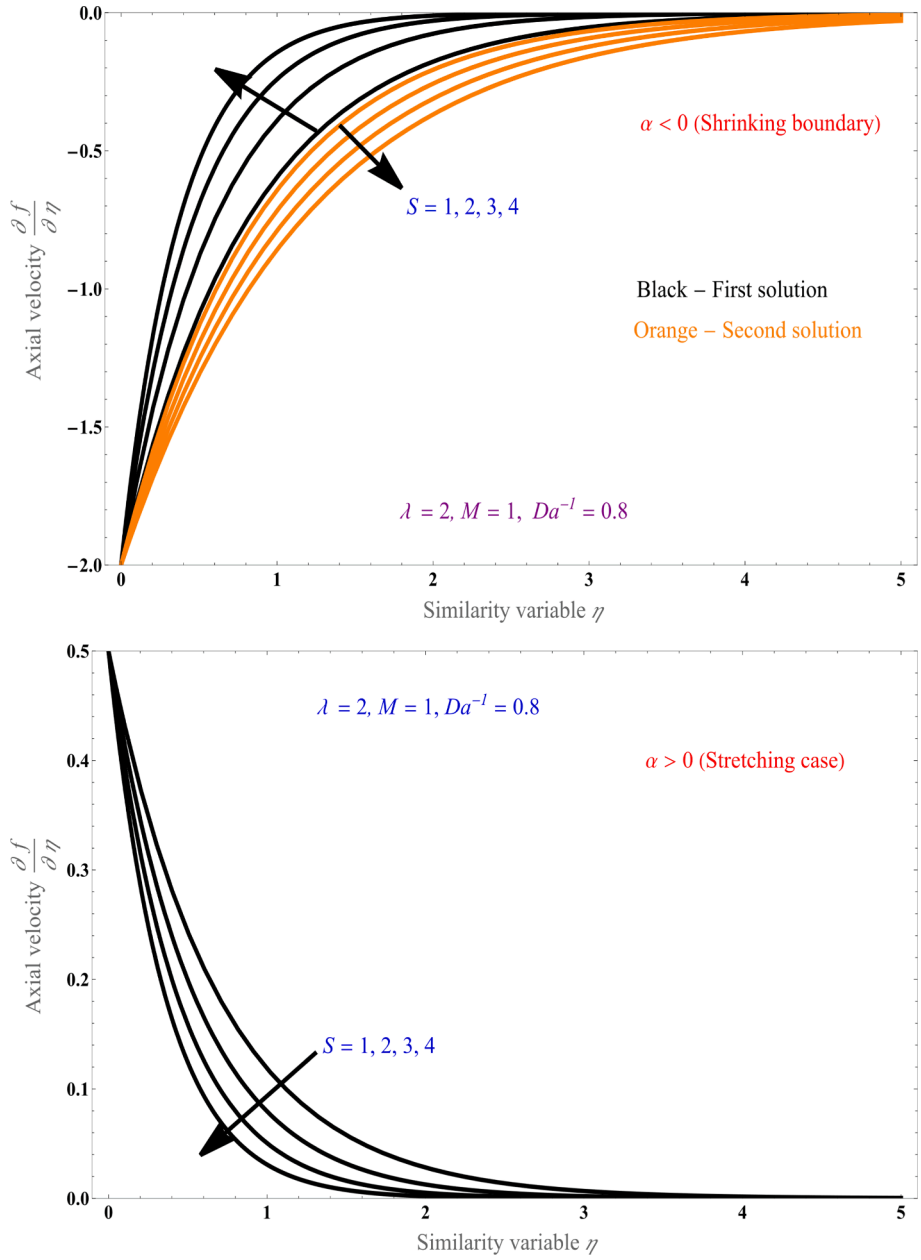

Fig. 14. (a): Graph of velocity with the similarity variable variation of *S*. (b): Graph of velocity with the similarity variable variation of *S*.

with the similarity variable, while keeping the Bingham fluid parameter, magnetic field, constant, the flow paths for the flow of the fluid are restricted due to improvement in the shape factor which exhibit frictional and drag force on the liquid. This results in a reduction in the improvement of velocity profile, the first graph shrinking boundary exhibits the dual solution showing the increasing of inverse Darcy number parameter increases the higher branch solution and lower branch solution. In the second graph for stretching boundary exhibits the unique solution and while raising the inverse Darcy number parameter the first branch solution shows increasing in nature. Darcy number parameter shows the increasing nature of stretching/shrinking boundary surface. Inverse Darcy parameters have a wide range of physical applications in various fields, including environmental remediation, fuel cell technology, and soil mechanics, and also porous materials can be used for sound absorption in buildings, bridges, highways, and subways for sound control.

Fig. 17 (a) & Fig. 17 (b) represent the graphs of the temperature profile with the similarity variable, while keeping the inverse Darcy number, magnetic field, and Biot number constant, taking the heat sink parameter and magnetic field as constant, The effects of the λ on the temperature fields are relatively higher compared with the effects on velocity distribution. The temperature boundary layer becomes thicker, and consequently, the thermal resistance is strengthened in the thermal boundary layer, the first graph shrinking boundary exhibits the dual solution showing the increasing of biviscosity Bingham fluid parameter increases the higher branch solution but the lower branch solution shows a decreasing nature. The second graph for the stretching boundary exhibits the unique solution and while raising the biviscosity Bingham fluid parameter increases the thermal boundary thickness. The biviscosity Bingham fluid parameter shows a similar nature for both stretching and shrinking surface. The Bingham parameter is used to describe the flow behavior of Bingham fluids. It is a useful tool in various industries, including oil and gas, food, printing, and medical industries.

Fig. 18 (a)&Fig. 18 (b) display the graphs of the temperature profile with the similarity variable, while keeping the inverse Darcy number, magnetic field, and Biot number constant, taking heat sink parameter

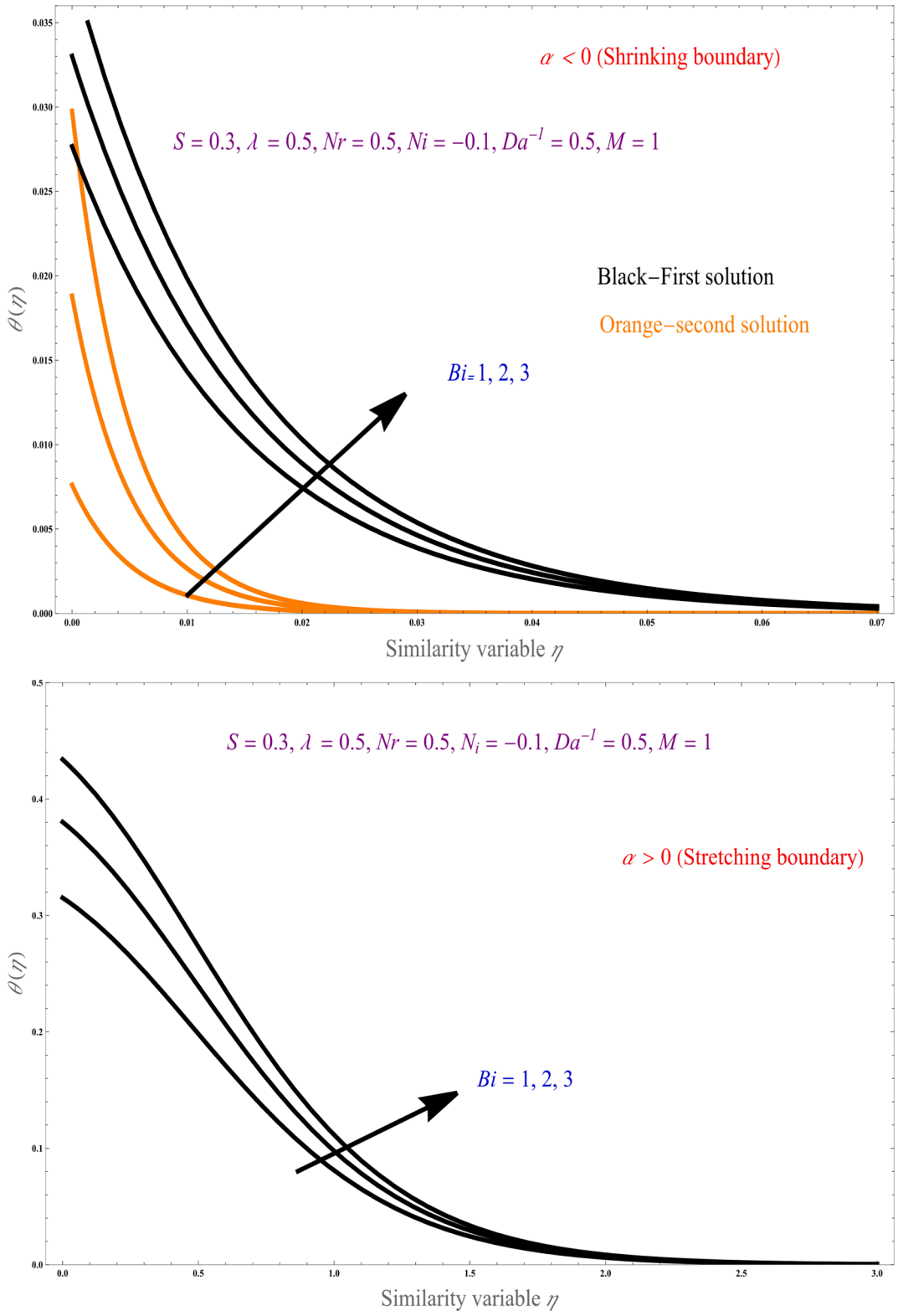

Fig. 15. (a): Graph of temperature with the similarity variable variation of Biot number. (b): Graph of temperature with the similarity variable variation of Biot number.

and magnetic field as constant, mass suction/injection refers to the process of introducing or removing fluid from a system through boundary surfaces, this process can significantly change the flow field and is applied to minimize energy losses by using the drag on the surface the first graph shrinking boundary exhibits the dual solution shows the increasing of mass suction/injection value increases the higher branch solution but lower branch solution shows decreasing nature. In the second graph for stretching boundary exhibits the unique solution and while raising the mass suction/injection value the first branch solution shows a decrease in nature. The mass suction/injection value shows a different nature for both stretching and shrinking surfaces. Mass transpiration has several applications in temperature control including

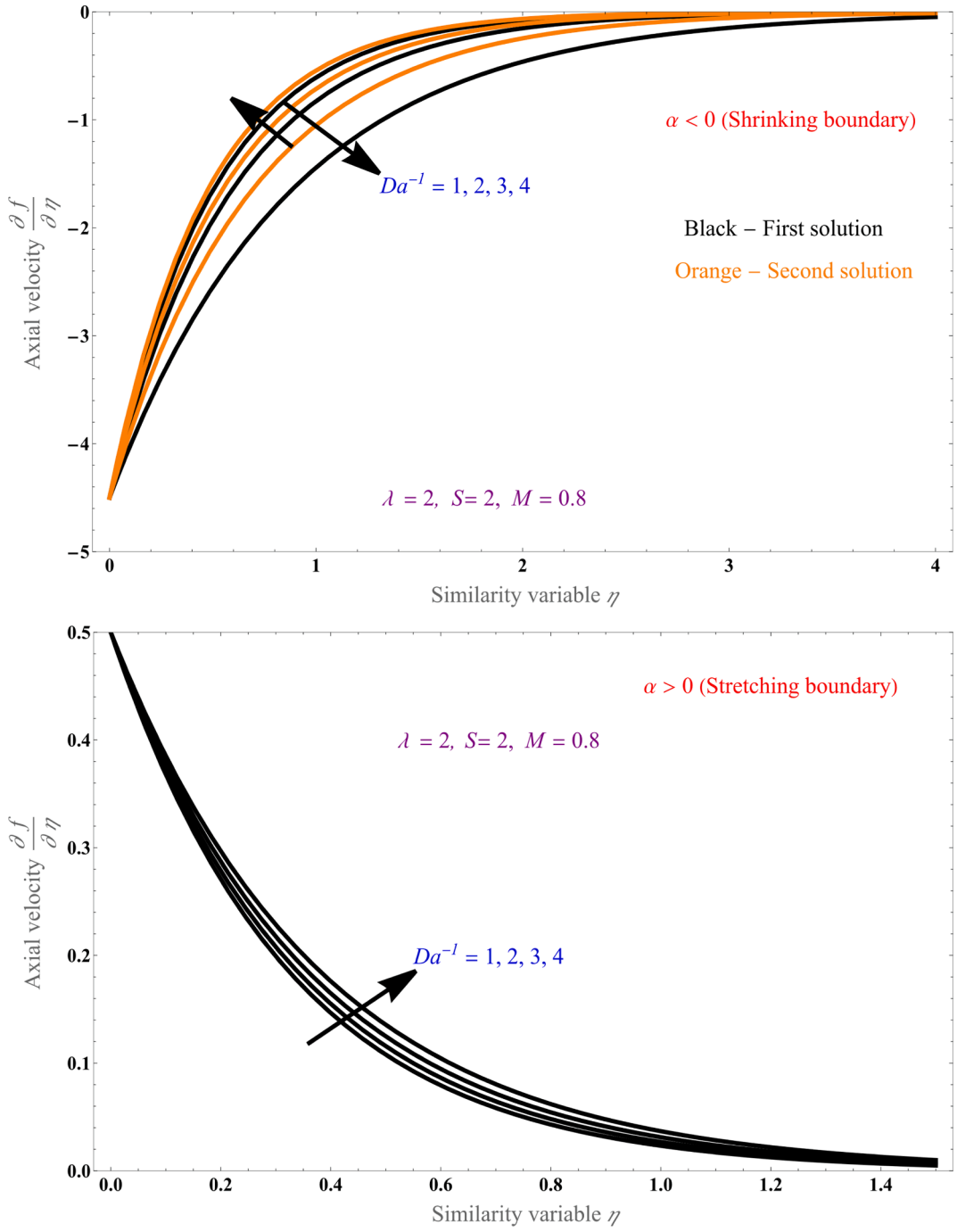

Fig. 16. (a): Graph of velocity with variation of Da^{-1}. (b): Graph of velocity with variation of Da^{-1}.

chemical processes, cooling, preventing corrosion or scaling, and reducing energy losses due to surface drag.

Fig. 19 (a) & Fig. 19 (b) represent the graphs of the temperature profile with the similarity variable while keeping inverse Darcy number, magnetic field, and Biot number constant, radiation parameter and magnetic field as constant, the parameter N_i refers to the amount of heat produced/consumed per unit volume. Internal heat generation/absorption improves the heat transfer, increase in heat source/sink increases the thickness of the thermal boundary layer. Increasing the heat source intensity corresponds to a greater thermal diffusion layer, presence of heat source limits in the flow state produces more heat, due to the production of energy in the thermal boundary layer, the first graph shrinking boundary exhibits the dual solution shows the increasing of heat source/sink parameter value increases the higher branch solution but lower branch solution shows decreasing nature. In the second graph for stretching boundary exhibits the unique solution and while raising the N_i parameter value, the first branch solution shows decreasing in nature. The N_i parameter value shows a different nature for both stretching and shrinking surfaces. Heat sources/sinks are commonly used in electronic devices to transfer the heat generated by high-power semiconductor devices such as power transistors and optoelectronics such as lasers and light-emitting diodes (LEDs) to a fluid medium, often air or a liquid coolant.

Fig. 20 (a) &Fig. 20 (b) represent the graphs of the temperature profile with the similarity variable while keeping the biviscosity Bingham fluid parameter, radiation parameter, and Biot number constant,

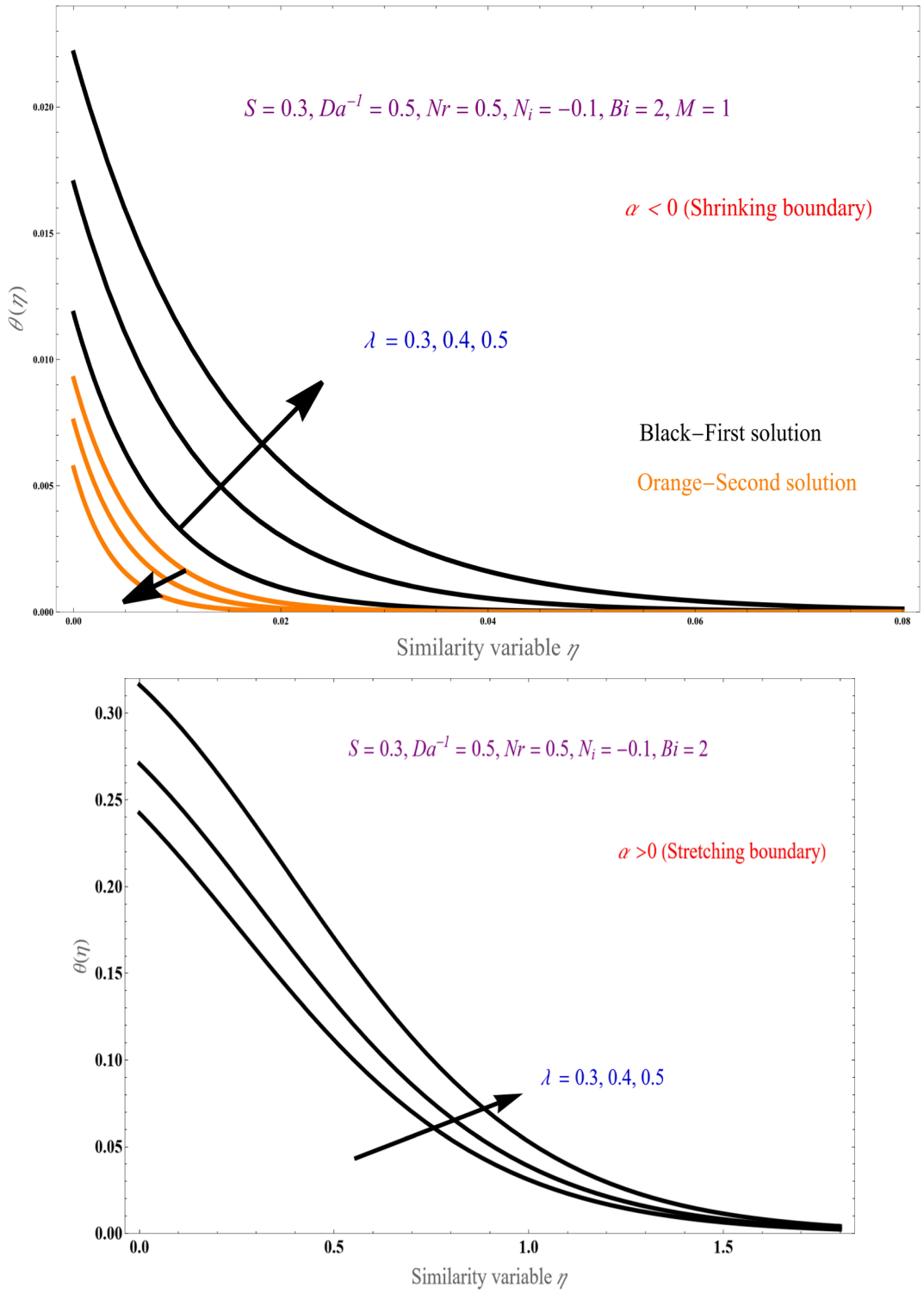

Fig. 17. (a): Graph of temperature with variation biviscosity Bingham parameter λ. (b): Graph of temperature with a variation of biviscosity Bingham parameter λ.

taking the heat sink parameter. Magnetic field encourages the resistive Lorentz force, which is present in an electrically conducting fluid. By this force results in resistance to the fluid particle's momentum which directly affects the temperature. Physically, an increase in the magnetic parameter makes it harder for the fluid to move, which naturally leads to a rise in the thermal rate, increasing the magnetic field raises the thermal boundary layer. The first graph shrinking boundary exhibits the dual solution and shows the increasing magnetic field increases the higher branch solution and increases the lower branch solution. The second graph for stretching boundary exhibits the unique solution and while raising the magnetic field parameter the first branch solution shows decreasing in nature. Magnetic field shows the increasing nature of stretching and shows reverse phenomena for shrinking boundary surfaces. The magnetic field has several applications in temperature control including, MHD-based micro-pumps, micro-coolers, micro-stirrers, and magnetohydrodynamic power plants, magnetic field has several biomedical applications, including magnetohydrodynamic-based laser beam scanning, nanoparticle manipulations for drug

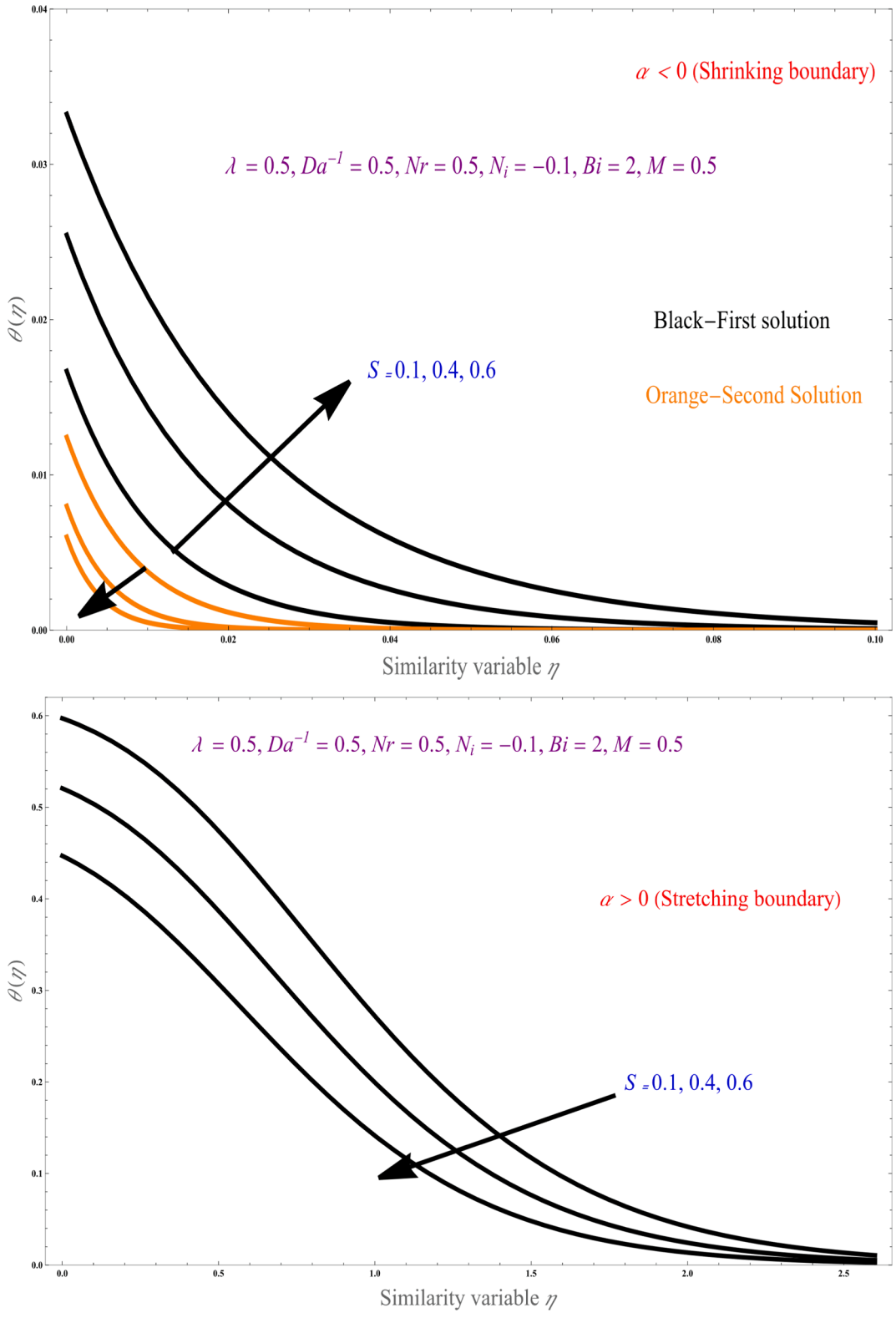

Fig. 18. (a): Graph of temperature with variation of *S*. (b): Graph of temperature with the similarity variable variation of *S*.

delivery.

Fig. 21 (a)&Fig. 21 (b) represent the graphs of the temperature profile with the similarity variable, while keeping the biviscosity Bingham fluid parameter, magnetic field, and inverse Darcy number constant, taking heat sink parameter and magnetic field and Biot number as constant, increases in radiation absorption throughout the boundary layer region the temperature of the fluid strengthens with reinforcement in time for both stretching/shrinking case, radiation behaves like a supporting force which accelerates the fluid particles near the vicinity of the plate. It is also noted that temperature boundary layer thickness increases when radiation tends to increase inside a boundary layer region, the first graph shrinking boundary exhibits the dual solution showing the increasing of radiation parameter increases the both higher branch solution and lower branch solution. The second graph for the

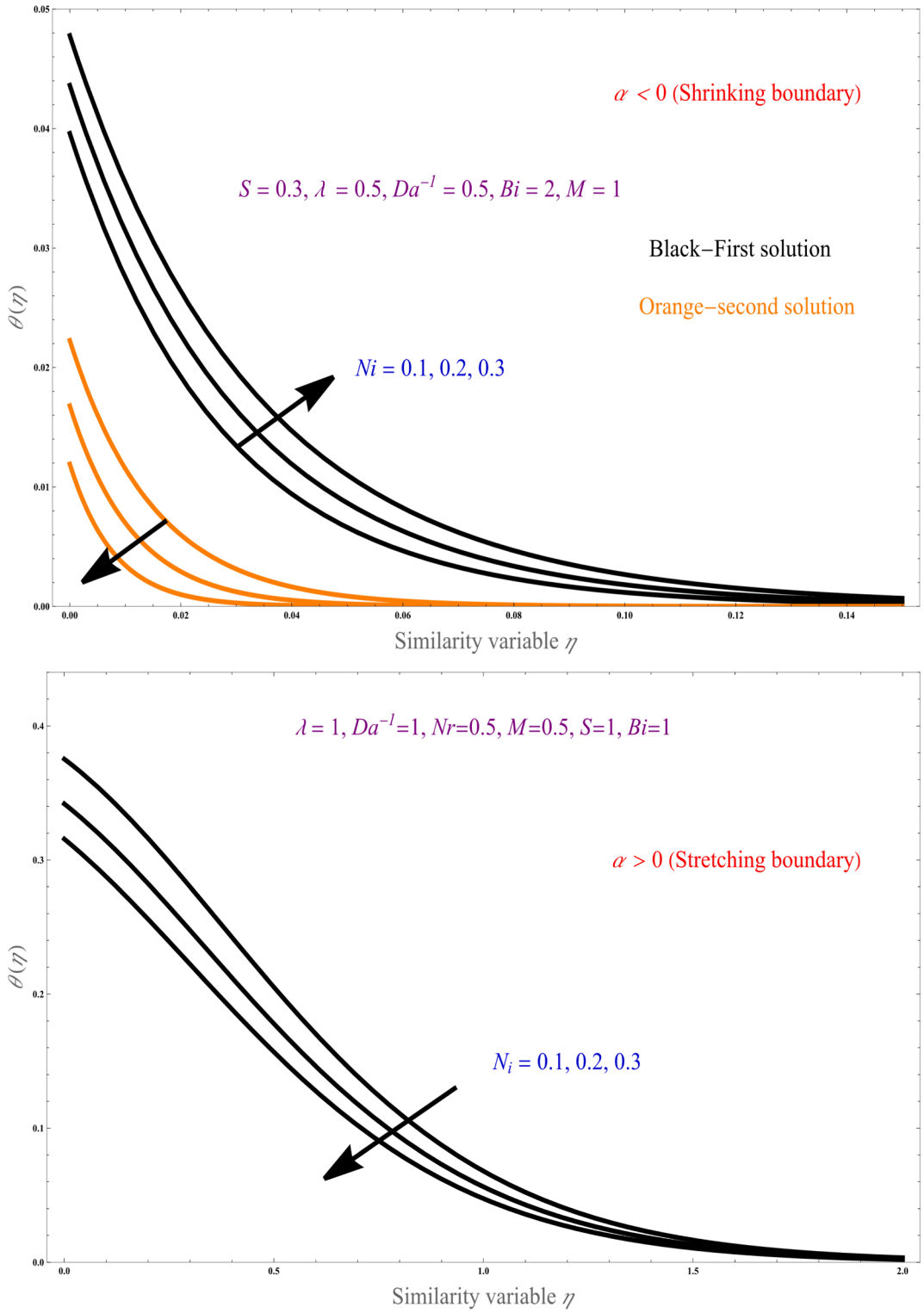

Fig. 19. (a): Graph of temperature with variation of N_i. (b): Graph of temperature with a variation of N_i.

stretching boundary exhibits the unique solution and while raising the radiation parameter the first branch solution shows increasing in nature, for the radiation parameter both graphs show an increasing nature of over-stretching and shrinking boundary surface. Thermal management: Thermal radiation is important for thermal management in various applications, including electronics, aerospace, and energy-conversion devices. Thermal radiation is used in spectroscopy to study the properties of materials and their interactions with electromagnetic radiation and is also used in thermal imaging to capture and display the infrared radiation emitted by objects.

Fig. 22 (a)&Fig. 22 (b) represent the graphs of the temperature profile with the similarity variable, while keeping the biviscosity Bingham fluid parameter, magnetic field, and inverse Darcy number constant, taking heat sink parameter and magnetic field and Biot number as constant, An increase in thermal conductivity with the volume fraction nanoparticles, also the thermal boundary layer thickness reduces with

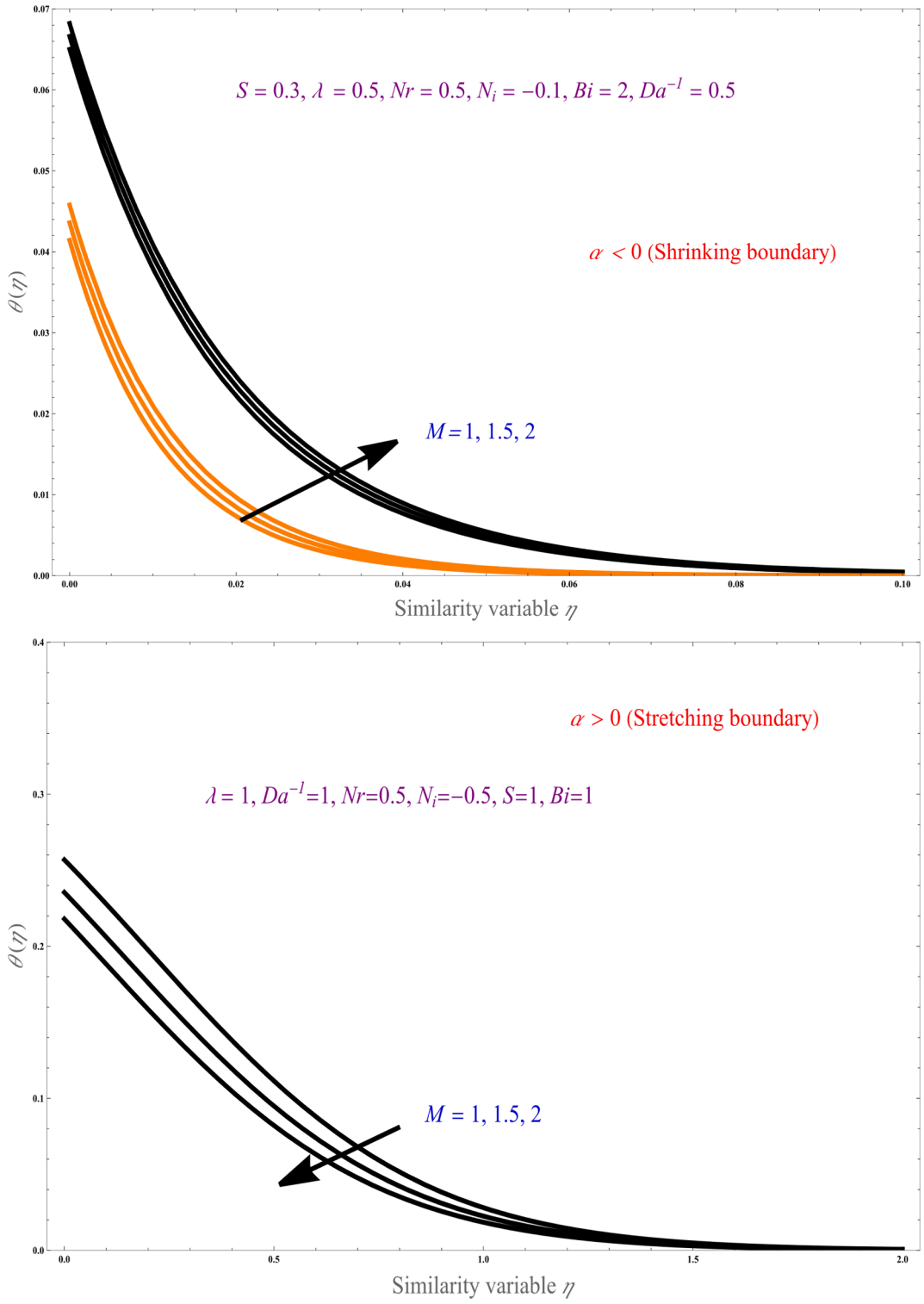

Fig. 20. (a): Graph of temperature with variation of magnetic field *M*. (b): Graph of temperature with a variation of *M*.

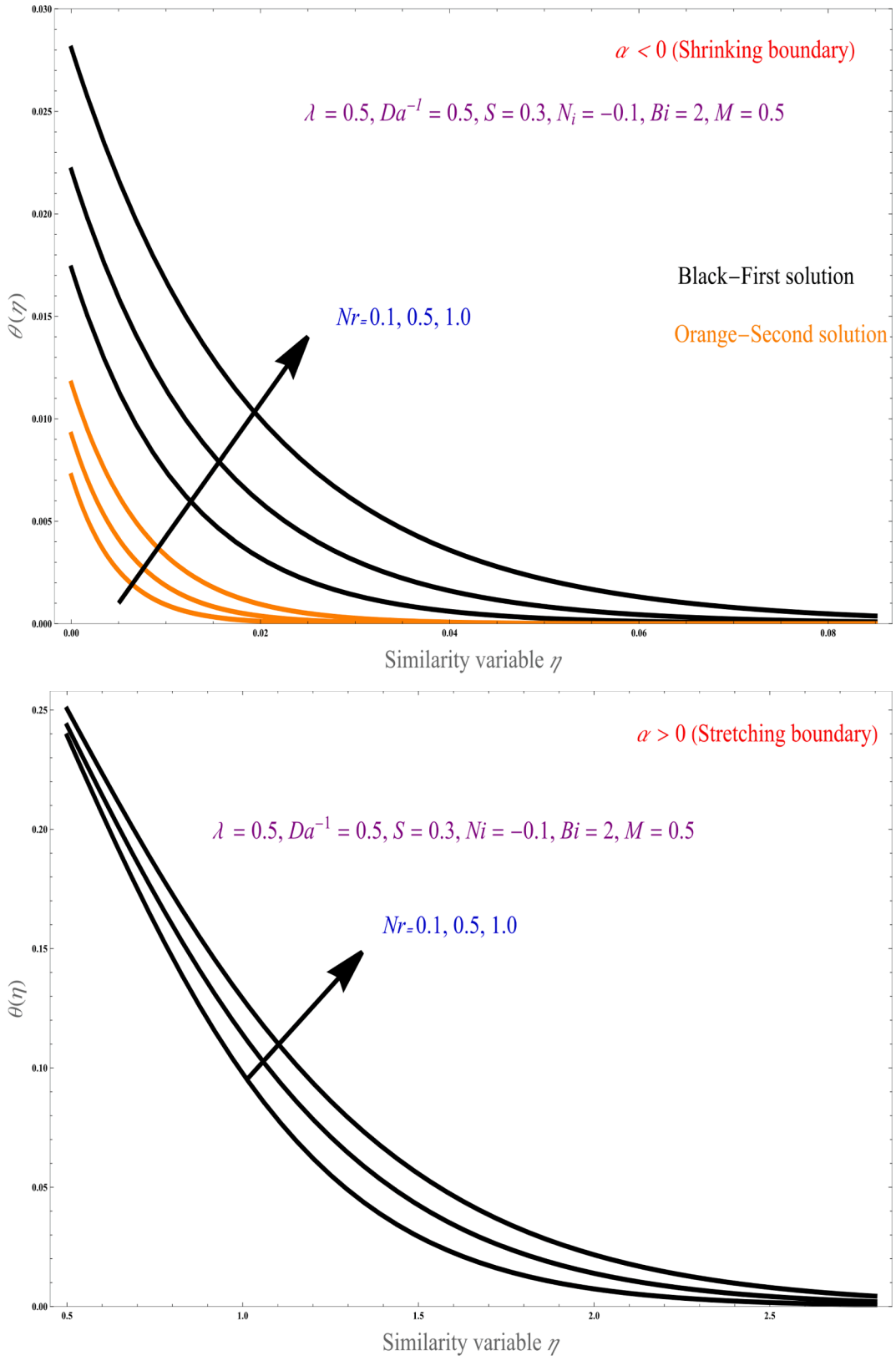

Fig. 21. (a): Graph of temperature with variation of *Nr*. (b): Graph of temperature with variation of *Nr*.

an amplify for nanoparticles thus the rate of heat transfer enhances with increases of volume fraction. The first graph shrinking boundary exhibits the dual solution shows the increasing of volume fraction parameter increases both higher branch solution and lower branch solution. The second graph for the stretching boundary exhibits the unique solution and while raising the volume fraction parameter the first branch solution shows increasing in nature, for the volume fraction parameter both graphs show the increasing nature over the stretching and shrinking boundary surface. Volume fraction feccet on temperature has several real-life applications, including wind engineering, making of

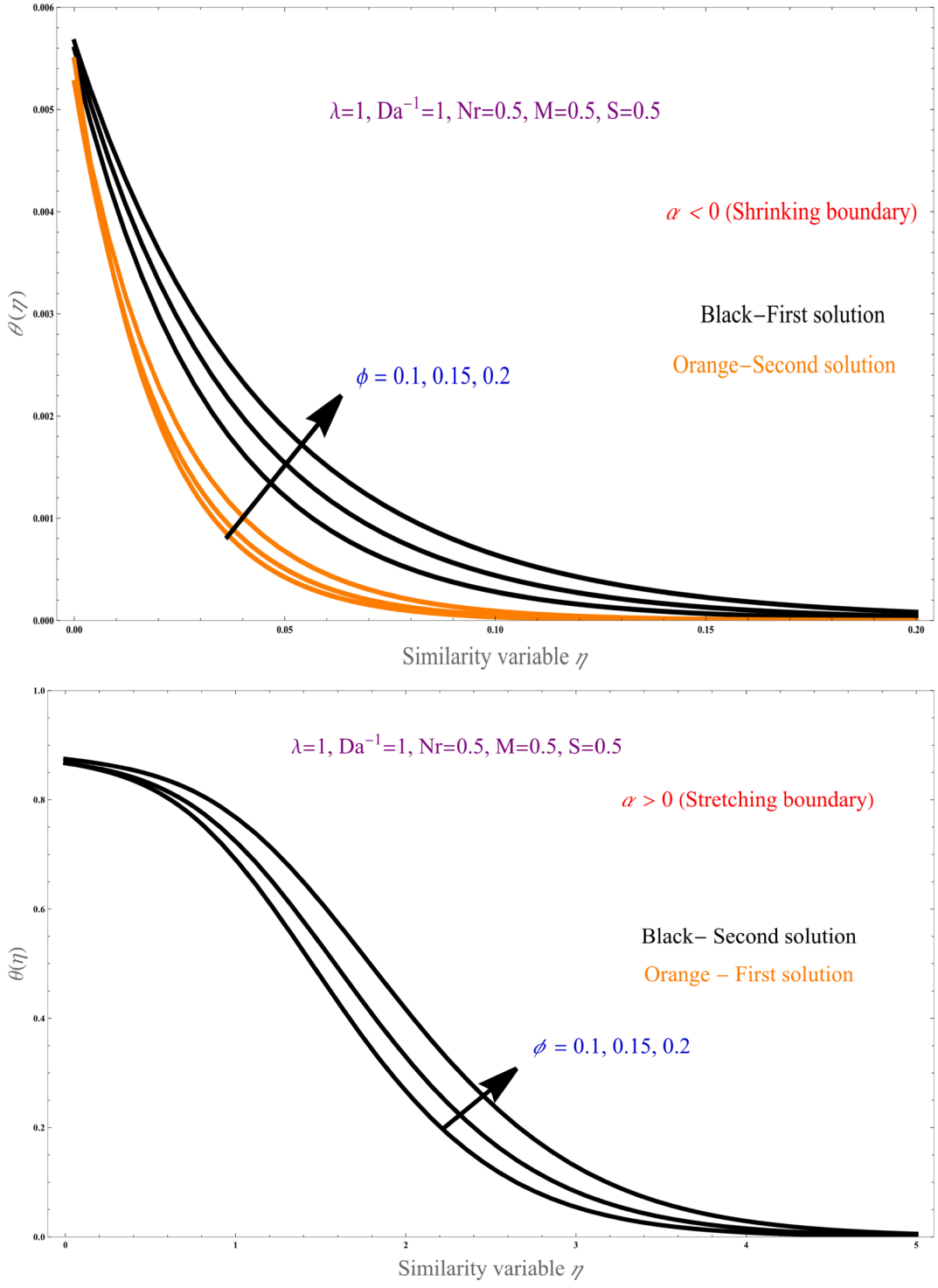

Fig. 22. (a): Graph of temperature with a variation of a ϕ. (b): Graph of temperature with variation of ϕ.

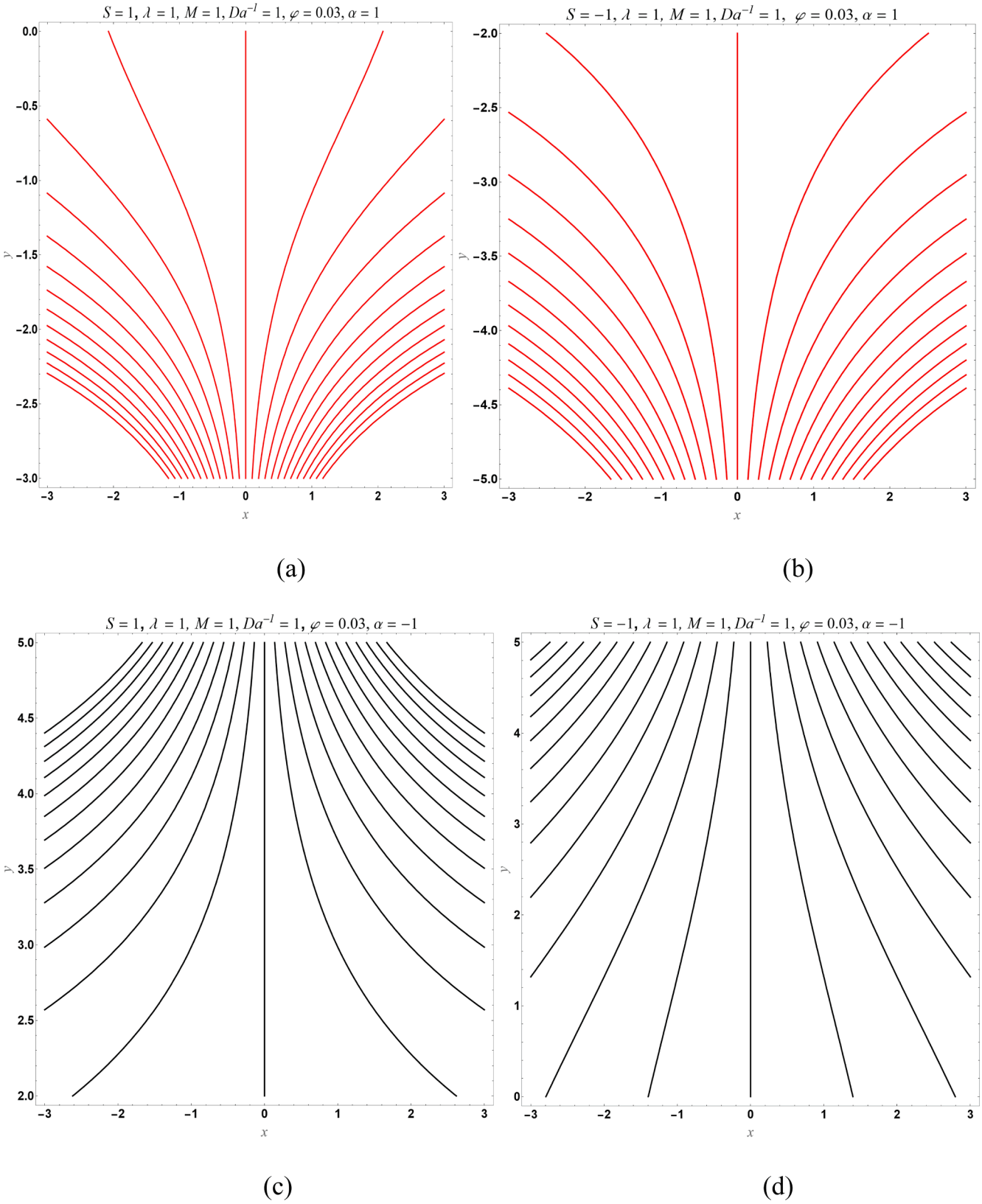

Fig. 23. Pattern of streamlines for cases: (a) suction for $\alpha > 0$ (b) injection for $\alpha > 0$ (c) suction for $\alpha < 0$(d) injection for $\alpha < 0$.

concrete mixtures, Material reconstructions, and mineral volume fraction determination technology.

Fig. 23 represents the streamlined graphs of the fluid flow, keeping all other parameters constant, graphs taken for both stretching and shrinking surface with the suction/injection cases. Streams line shows increasing nature for stretching surface and shows reverse phenomena for shrinking surface.

8. Conclusion of remark

Through the investigation of the present work, we study the influence of inclined magnetic field over the hybrid nanofluid with biviscosity Bingham fluid parameter over the porous medium and radiation also taken into account. By using suitable transformations, we convert velocity and temperature equations to the set of feasible ODEs form after that we solve by analytical method, physical significance parameters like radiation, heat source/sink, inverse Darcy number, Biot number, biviscosity Bingham fluid parameter have been examined.

The following points are observed in the current work.

- The variation of mass suction and α parameter with solution domain β while keeping all other parameters constant, we observe that an increase in α parameter will increase domain β in the higher branch.
- While increasing the magnetic field parameter skin friction also increases.
- Both solutions of skin friction coefficient for biviscosity Bingham parameter across the surface were found larger for mass suction and mass injection case.
- In the velocity profile, the first solution of magnetic field and mass suction/injection parameter shows the increasing nature for the shrinking case and shows decreasing nature over the stretching boundary.
- In the momentum profile graph, the higher solution of biviscosity Bingham fluid parameter shows the rising nature for both shrinking and stretching boundary.
- In the temperature profile, the first solutions of the volume fraction parameter, Biot number, and radiation parameter show the increasing nature in both stretching/shrinking boundary surfaces.
- In the temperature profile, the first solutions of mass suction/injection, heat Source/sink, and magnetic field parameter show increasing in shrinking surface and different phenomena over stretching surface.

CRediT authorship contribution statement

U.S. Mahabaleshwar: Supervision, Software, Resources, Investigation. **S.M. Sachhin:** Writing – original draft, Methodology, Formal analysis. **L.M. Pérez:** Writing – review & editing, Visualization, Software, Validation. **H.F. Oztop:** Writing – review & editing, Software, Resources.

Declaration of competing interest

The authors declare that they have no known competing financial interests or personal relationships that could have appeared to influence the work reported in this paper.

Data availability

No data was used for the research described in the article.

Acknowledgments

LMP acknowledges financial support from ANID through Convocatoria Nacional Subvención an Instalación en la Academia Convocatoria Año 2021, Grant SA77210040.

References

[1] S.U. Choi, J.A. Eastman, Enhancing Thermal conductivity of fluids with nanoparticles, Argonne National Laboratory. Illinois, IL, USA, 1995.
[2] G. Huminic, A. Huminic, The heat transfer performances and entropy generation analysis of hybrid nanofluids in a flattened tube, Int. National J. Heat and Mass Transfer. 57 (2018) 813–827.
[3] P.K. Das, A review based on the effect and mechanism of thermal conductivity of normal nanofluids and hybrid nanofluids, J. Mol. Liq. 240 (2017) 420–446.
[4] S. Suresh, K.P. Venkitaraj, M.S. Hameed, J. Sarangan, Turbulent heat transfer and pressure drop characteristics of dilute water-based Al_2O_3-Cu hybrid nanofluids, J. Nanosci. Nanotechnol. 14 (2014) 2563–2572.
[5] F.R. Siddiqui, C.Y. Tso, K.C. Chan, S.C. Fu, C.Y. Chao, On trade-off for dispersion stability and thermal transport of Al_2O_3-Cu hybrid nanofluid for various mixing ratios, Int. J. Heat Mass Transf. 132 (2019) 1200–1216.
[6] U.S. Mahabaleshwar, R. Mahesh, F. Sofos, Thermosolutal marangoni convection for hybrid nanofluid models: an analytical approach, Phys. 5 (2022) 24–44.
[7] S. Rostami, D. Toghraie, B. Shobhani, N. Sina, P. Barnoon, Measurement of the thermal conductivity of MWCNT-CuO/water hybrid nanofluid using artificial neural networks, J. Therm. Anal. Calorim. 143 (2021) 1097–1105.
[8] A.B. Vishalakshi, U.S. Mahabaleshwar, D. Laroze, D. Zeidan, A Study of mixed convective Ternary Hybrid nanofluid flow over a stretching sheet with radiation and transpiration. special topics and reviews in porous media, An Int. J. 14 (2023) 33–51.
[9] H. Yarmand, S. Gharehkhani, G. Ahmadi, Graphene nanoplatelets-silver hybrid nanofluids for enhanced heat Transfer, Energy Conversion Management. 100 (2015) 419–428.
[10] J. Ranga Babu, K.K. Kumar, S. Srinivas Rao, State-of-art review on hybrid nanofluids, Renew. Sustain. Energy Rev. 77 (2017) 551–565.
[11] D. Ingham, I. Pop, Transport Phenomena in Porous Media III, Elsevier, Oxford, 2005.
[12] T. Maranna, S.M. Sachhin, U.S. Mahabaleshwar, M. Hatami, Impact of Navier's slip and MHD on laminar boundary layer flow with heat transfer for non-Newtonian nanofluid over a porous media, Sci. Rep. 13 (1) (2023), https://doi.org/10.1038/s41598-023-39153-y.
[13] A. Kasaeian, R. Daneshazarian, O. Mahian, L. Kolsi, I. Pop, Nanofluid flow and heat transfer in porous media: a review of the latest developments, Int. J. Heat Mass Transfer. 107 (2017) 778–791.
[14] N.K. Mishra, P. Muthukumar, S.A. Panigrahy, A review on clean combustion within porous media, Book Chapter. Air Pollution and Control. (2018) 209–224.
[15] J.R. Howel, M.J. Hall, J.L. Ellzey, Combustion of hydrocarbon fuels within porous inert media, Prog. Energy Combust. Sci. 22 (1996) 121–145.
[16] D. Broseta, F. Medjahed, J. Lecourtier, Polymer adsorption/retention in porous media: effects of core wettability on residual oil, Spe Adv. Technol. 3 (1995) 103–112.
[17] P.X. Jiang, X.C. Lu, Numerical simulation of fluid flow and convection heat transfer in sintered porous plate channels, Int. J. Heat Mass Transf. 49 (2006) 1685–1695.
[18] S.M. Sachhin, U.S. Mahabaleshwar, H.-N. Huang, B. Sunden, D. Zeidan, An influence of temperature jump and Navier's slip-on hybrid nanofluid flow over a permeable stretching/shrinking sheet with heat transfer and inclined MHD, Nanotechnol. 35 (11) (2023) 115401, https://doi.org/10.1088/1361-6528/ad13be.
[19] M. Astanina, M. Sheremet, U.S. Mahabaleshwar, J. Singh, Effect of porous medium and copper heat sink on cooling heat-generating element, Energies. 13 (2020) pp2538.
[20] M. Hamid, M. Usman, Z.H. Khan, R. Ahmad, W. Wang, Dual solutions and stability analysis of flow and heat transfer of Bingham fluid over the stretching sheet, Phys. Lett. A. 1 (258) (2019) 1–9.
[21] M.R. Khan, M.A. Elkotb, R.T. Matoog, N.A. Alshehri, A.H. Mostafa, Thermal features and heat transfer enhancement of a Bingham fluid across a porous stretching/shrinking sheet: analysis of dual solutions, Case Studies in Thermal Eng. 28 (2021) 101–115.
[22] K.A. Khan, F. Jamil, J. Ali, I. Khan, N. Ahmed, M. Rafiq, Analytical simulation of heat and mass transmission in bingham fluid flow across a stretching surface, Math. Probl. Eng. 11 (2022) 205–216.
[23] I.C. Liu, A note on heat and mass transfer for a hydromagnetic flow over a stretching sheet, Int. Communication Heat and Mass Transfer. 32 (2005) 1075–1084.
[24] U.S. Mahabaleshwar, K.R. Nagaraju, P.N. Vinaykumar, Effect of radiation on thermosolutal Marangoni convection in a porous medium with chemical reaction and heat source/sink, Physics of Fluid. 32 (2020) 550–602.
[25] R. Mahesh, U.S. Mahabaleshwar, P.N. Vinaykumar, H.F. Oztop, Impact of radiation on the MHD couple stress hybrid nanofluid flow over a porous sheet with viscous dissipation, Results in Eng. 17 (2023) 100–113.
[26] V.S. Reddy, J. Kandasamy, S. Sivanandam, Impacts of Casson Model on Hybrid Nanofluid flow over a moving thin needle with Dufour and Soret and thermal radiation effects, Mathematical and Computational Applications. 28 (2022) 2–15.
[27] M. Arif, P. Kumam, W. Kumam, I. Khan, M. Ramzan, A fractional model of Bingham fluid with ramped wall temperature: engineering applications of engine oil, Computational and Mathematical Methods. 3 (2021) 6–12.
[28] A. Raza, S. Ullah Khan, K. Al-Khaled, M. Ijaz Khan, A. Ul Haq, F. Alotaibi, A.A. A. Mousa, S. Qayyum, A fractional model for the kerosene oil and water-based Casson nanofluid with inclined magnetic force, Chem. Phys. Lett. 787 (2022) 139277.
[29] N. Manzoor, I. Qasim, M.I. Khan, M.W. Ahmed, K. Guedri, O.T. Bafakeeh, E.S. M. Tag-Eldin, A.M. Galal, Antibacterial applications of low-pressure plasma on

degradation of multidrug-resistant V. cholera, Appl. Sci. 12 (2022) 9737, https://doi.org/10.3390/app12199737.
[30] Usman, M.I. Khan, F. Shah, S.U. Khan, A. Ghaffari, Y.-M. Chu, Heat, and mass transfer analysis for the bioconvective flow of Eyring Powell nanofluid over a Riga surface with nonlinear thermal features, Numer. Methods Partial Differ. Equ. 38 (2022) 777–793, https://doi.org/10.1002/num.22696.
[31] M. Ijaz Khan, F. Alzahrani, Numerical simulation for the mixed convective flow of non-Newtonian fluid with activation energy and entropy generation, Math. Methods Appl. Sci. 44 (2021) 7766–7777, https://doi.org/10.1002/mma.6919.
[32] U.S. Mahabaleshwar, T. Maranna, F. Sofos, Analytical investigation of an incompressible viscous laminar Bingham fluid flow past a stretching/shrinking sheet, Sci. Rep. 12 (2022) 18404.
[33] U. Khan, A. Zaib, A. Ishak, N.C. Roy, S.A. Bakar, T. Muhammad, A.H.A. Aty, I. S. Yahia, Exact solutions for MHD axisymmetric hybrid nanofluid flow and heat transfer over a permeable non-linear radially shrinking/stretching surface with mutual impacts of thermal radiation, European Physical J. Special Topics. 231 (2022) 1195–1204.
[34] R. Mahesh, U.S. Mahabaleshwar, P.N.V. Kumar, H.F. Öztop, N. Abu-Hamdeh, Impact of radiation on the NHD couple stress hybrid nanofluid flow over a porous sheet with viscous dissipation, Results in Eng. 17 (2023) 100905.
[35] F. Selimefendigil, H.F. Öztop, Combined effects of using multiple porous cylinders and inclined magnetic field on the performance of hybrid nano liquid forced convection, J. Magn. Magn. Mater. 565 (2023) 170137.
[36] M.M. Bhatti, H.F. Öztop, R. Ellahi, Study of magnetized hybrid nanofluid flow through a flat elastic surface with applications in solar energy, Mater. 15 (2022) 7507.
[37] M. Nazeer, F. Hussain, M.I. Khan, K. Khalid, Theoretical analysis of electrical double layer effects on the multiphase flow of Jeffrey fluid through a divergent channel with lubricated walls, Waves Random Complex Media. (2022) 1–15, https://doi.org/10.1080/17455030.2022.2126025.
[38] M. Khan, S. Qayyum, S. Kadry, W. Khan, S. Abbas, Theoretical investigations of entropy optimization in electro-magneto nonlinear mixed convective second order slip flow, J. Magn. 25 (2020) 8–14, https://doi.org/10.4283/JMAG.2020.25.1.008.
[39] M.I. Khan, F. Alzahrani, Transportation of heat through Cattaneo-Christov heat flux model in non-Newtonian fluid subject to internal resistance of particles, Appl. Math. Mech. 41 (2020) 1157–1166, https://doi.org/10.1007/s10483-020-2641-9.
[40] D. Ramesh, et al., Computational analysis on radiative non-Newtonian Carreau nanofluid flow in a microchannel under the magnetic properties, Sci. Iran. 30 (2023) 376–390, https://doi.org/10.24200/SCI.2022.58629.5822.
[41] F. Mebarek-Oudina, et al., Hydromagnetic flow of magnetite-water nanofluid utilizing adapted Buongiorno model, Int. J. Mod Phys B. 38 (2024) 2450003, https://doi.org/10.1142/S0217979224500036.